NASA Technical Memorandum

NASA TM - 103591

LINEAR ELASTIC FRACTURE MECHANICS PRIMER

By C.D. Wilson

Structures and Dynamics Laboratory
Science and Engineering Directorate

July 1992

National Aeronautics and Space Administration

George C. Marshall Space Flight Center

PREFACE

Today's structural engineers are well–acquainted with using strength of materials concepts and the finite element method for stress analysis. Additionally, most structural engineers have a working knowledge of the fatigue behavior of metals. Unfortunately, the application of fracture mechanics is not as well understood. Fracture analyses are often performed using computer software (**NASA/FLAGRO** [1] [1] and **NASCRAC** [2] for example) as a "black box." This primer is intended to remove the blackbox perception by introducing linear elastic fracture mechanics (LEFM) and fracture control based on LEFM.

This primer began with the notes from two graduate courses at Tennessee Technological University: "Mechanics of High–Strength Materials" and "Fracture Mechanics" taught by Dallas Smith of the Department of Civil Engineering. The author's research interest in fracture mechanics was fostered by his graduate advisor, Dale Wilson of the Department of Mechanical Engineering. After joining the George C. Marshall Space Flight Center, the author was inspired by Gwyn Faile of the Durability Analysis Branch to promote the development of fracture mechanics tools for the practicing engineer. The notes from the course "SSME Fracture Mechanics," taught by Dale Russell and his associates at the Rocketdyne Division of Rockwell International Corporation, were invaluable to the author. The author thanks Preston McGill of the Metallurgy Research Branch and George Pinkas of Lewis Research Center for the photographs used in this primer. The author also thanks the many people who reviewed drafts of this primer.

C.D. Wilson

Huntsville, Alabama
July 1992

[1] The numbers in brackets refer to the list of references at the end of this paper.

TABLE OF CONTENTS

LIST OF ILLUSTRATIONS

LIST OF TABLES

TECHNICAL MEMORANDUM

LINEAR ELASTIC FRACTURE MECHANICS PRIMER

1 INTRODUCTION

1.1 Recommended Reading

There are many excellent textbooks on fracture mechanics. Unfortunately, most structural engineers do not have the time to read these textbooks. Many references are included to assist the reader in discovering more details about fracture mechanics. A list of recommended texts for additional reading is:

- "Elementary Engineering Fracture Mechanics" by D. Broek [3]
- "Fracture Mechanics" by H.L. Ewalds and R.J.H. Wanhill [4]
- "Fracture Mechanics: Fundamentals and Applications" by T.L. Anderson [5]
- "Failure of Materials in Mechanical Design: Analysis, Prediction, Prevention" by J.A. Collins [6]
- "Fundamentals of Metal Fatigue Analysis" by J.A. Bannantine, J.J. Comer, and J.L. Handrock [7]
- "Understanding How Components Fail" by D.J. Wulpi [8].

1.2 Historical Perspective

In 1913, C.E. Inglis [9] published a mathematical analysis for the stresses in the region of an elliptical hole in a two-dimensional finite plate, modeled a crack as a slender elliptical opening, and estimated stress concentrations for various geometries. In the early 1920's, A.A. Griffith [10] used the work of Inglis to formulate an energy criterion for predicting if a crack would unstably propagate in an ideally brittle material, resulting in failure. If the rate of change in the elastic energy stored in the plate equaled or exceeded the work required to produce new fracture surface, then crack extension occurred.

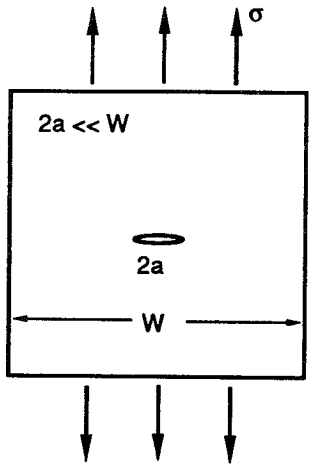

Figure 1. Griffith's flaw model.

Griffith's model was a straight through the thickness crack [2] of length $2a$ in a large rectangular plate loaded with a nominal stress of σ as shown in Figure 1. Griffith calculated the change in elastic strain energy U stored in the uncracked plate and the energy stored in the cracked plate with two crack tips when the load on the plate remains constant:

$$U = \frac{\pi\sigma^2 a^2}{E}, \tag{1}$$

where E is the Young's modulus. Griffith calculated the rate at which the plate converts strain energy into energy required for crack extension at a single crack tip, G_I, is:

$$G_I = \frac{dU}{da} = \frac{\pi\sigma^2 a}{E}. \tag{2}$$

The dimensions of elastic strain energy release rate G_I [3] are FL/L^2 (work per unit area). G_I is also called the crack driving force because its dimensions can be expressed as F/L (force per unit length).

[2] A straight through the thickness crack is commonly denoted as a "through crack."

[3] The subscript I refers to the opening mode of crack–tip deformation. Further explanation is given in section 2.

As G_I approaches a critical value G_c, unstable crack extension is assumed to occur. The critical stress can be determined by letting $G_I \rightarrow G_c$ in equation 2 and solving for σ_c:

$$\sigma_c = \sqrt{\frac{EG_c}{\pi a}}. \tag{3}$$

The critical stress is proportional to $a^{-1/2}$. The critical strain energy release rate G_c is a constant for a given material and must be determined experimentally. G_c can be viewed as the material's resistance to crack extension. In his experiments with glass, Griffith assumed that the material's resistance was due to its surface energy γ, similar to the surface tension of a liquid. G_c would be twice the surface energy ($G_c = 2\gamma$) because two new surfaces are formed during crack extension.

In the late 1940's, G.R. Irwin [11] and E. Orowan [12] showed that G_c for metals is due to yielding and plastic deformation around the advancing crack tip rather than surface energy. In fact, the surface energy for most metals is so small compared with the plastic work that it can be neglected. Therefore, ignoring the plastic work component of G_c severely underestimates the fracture strength of metals.

The energy approach has been largely replaced by a stress intensity factor (K_I) [4] approach developed by Irwin [13] and M.L. Williams [14] in the 1950's. Irwin showed that fracture occurs when a critical stress distribution ahead of the crack tip is reached. The stress intensity factor for the Griffith problem is:

$$K_I = \sigma\sqrt{\pi a}. \tag{4}$$

There is a simple relationship between the stress intensity factor K_I approach and the energy release rate G_I approach. Both sides of equation 4 are squared, and the resulting expression is divided by E, and then combined with equation 2:

$$\frac{K_I^2}{E} = \frac{\pi\sigma^2 a}{E} = G_I. \tag{5}$$

The above equation can be more generally stated:

$$G_I = \frac{K_I^2}{E'}, \tag{6}$$

[4]The stress intensity factor was denoted by the symbol K in honor of J.A. Kies, a collaborator of Irwin's at the Naval Research Laboratory. The strain energy release rate was denoted by the symbol G in honor of A.A. Griffith.

where $E' = E$ for plane stress and $E' = E/(1-\nu^2)$ for plane strain [5] (ν is Poisson's ratio). If G_I approaches its critical value, then K_I approaches its critical value.

P.C. Paris [15] applied fracture mechanics to the problem of fatigue in metals in 1961. He noted that the rate of fatigue crack growth was related to the stress intensity factor range of the applied load cycles. By the early 1960's, fracture mechanics was firmly established as a useful tool in preventing the failure of structures due to crack–like defects.

1.3 Significance of Fracture Mechanics

The simplest way to establish the significance of the fracture mechanics approach is to compare it to the strength of materials approach. In the strength of materials approach, the applied stress is compared to the yield or ultimate strength of the material. In the fracture mechanics approach, the applied stress must be combined with an appropriate flaw size and then compared to the critical stress intensity factor. For example, the critical pressure for a thin–walled pressure vessel can be determined using both approaches. For the strength of materials approach, the hoop stress must be less than the yield strength:

$$\sigma = \frac{pR}{t} < \sigma_{ys}. \tag{7}$$

The critical pressure based on yield is:

$$p_{yield} = \sigma_{ys}\left(\frac{t}{R}\right). \tag{8}$$

For the fracture mechanics approach, the stress intensity factor, K_I, must be less than the critical stress intensity factor, K_c:

$$K_I = \sigma\sqrt{\pi a} = \frac{pR}{t}\sqrt{\pi a} < K_c. \tag{9}$$

The critical pressure based on fracture is:

$$p_{fracture} = \frac{K_c}{\sqrt{\pi a}}\left(\frac{t}{R}\right), \tag{10}$$

[5] The terms "plane stress" and "plane strain" are explained in detail in section 2.3.

where a is the largest flaw size that could exist undetected in the vessel. The fracture mechanics approach governs the design when $p_{fracture} < p_{yield}$. If this situation occurs, ignoring fracture mechanics can easily lead to an unexpected failure.

Most structures contain defects or crack–like flaws. Structures made from brittle materials are seriously affected because their strength is severely reduced by the stress concentration near a crack. The high–strength, low–density metallic alloys used in aerospace structures can be very flaw–sensitive. For this reason, fracture mechanics was largely developed in the aerospace industry. However, its principles are widely used in many other industries.

The possibility of brittle fracture occuring in a structure made from a high–strength, flaw–sensitive material exists even when working stresses are well below the yield strength. Brittle fracture from crack–like flaws can be catastrophic and can occur with little advance warning, unlike ductile failure which usually requires noticeable deformation and distortion. The crack–like flaws may originate from inclusions and voids inherent in the material; fabrication processes like welding and heat treatment; and mishandling of tools causing scratches or dents. Fatigue cracks can initiate from these defects, as well as from other stress concentrations at fillets and holes. Failures from brittle fracture have compelled engineers to design structures which will tolerate flaws large enough to be detected by nondestructive inspection before the flaws can grow to critical size.

Fracture mechanics deals with the residual strength and remaining life of a structure which contains a crack. The engineering problem of a crack in a structure shown in Figure 2 leads to these questions:

- What is the residual strength of a structure as a function of crack size?
- What is the maximum permissible crack size that a structure can tolerate?
- How long does it take for a crack to grow from its initial size to the maximum permissible size?
- What is the service life of a structure when a certain preexisting flaw size is assumed to exist?
- During the period available for crack detection, how often should a structure be inspected for cracks? [3]

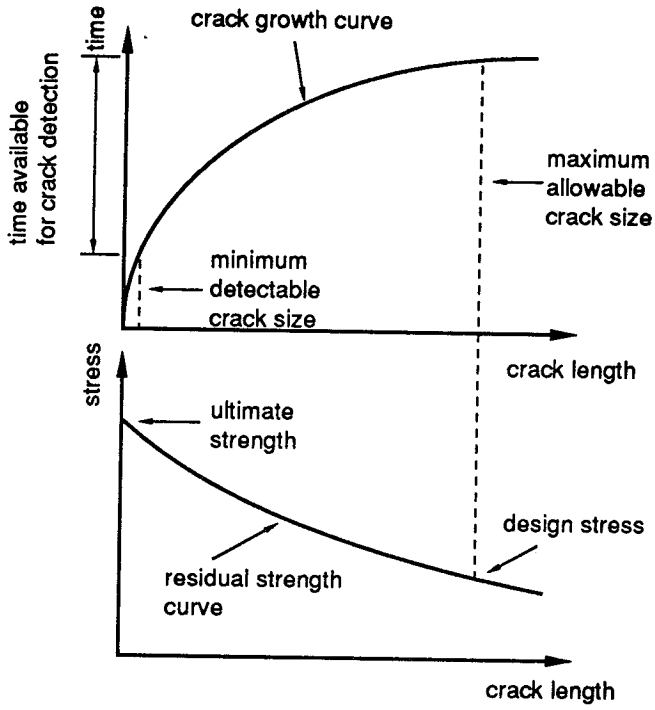

Figure 2. Engineering problem of a crack in a structure.

2 CRACK–TIP STRESSES

2.1 Modes of Crack–Tip Deformation

Cracks in structures may be irregular in shape and may be subjected to complex loadings. The resulting deformation of the material around the crack tip, where further crack growth begins, may be complex. Three fundamental modes of crack–tip deformation are required to describe the general state of deformation near the crack tip. For mode I, the "opening" mode, the crack surfaces are displaced normal to the crack plane. Inplane shear stresses cause mode II, the "sliding" mode, where the crack surfaces are displaced in the crack plane in a direction analogous to an edge dislocation. Out–of–plane shear stresses cause mode III, the "tearing" mode, where the crack surfaces are displaced in the crack plane in a direction analogous to a screw dislocation. The subscripts I, II, and III are used to denote the particular mode. The general deformation may be viewed as a combination of the three modes of deformation shown in Figure 3. In cases of combined loading, modes II and III may influence crack growth, causing the crack to change its initial direction and grow normal to the applied stress in the opening mode. Therefore, mode I is the fracture mode of most significant practical interest. [3]

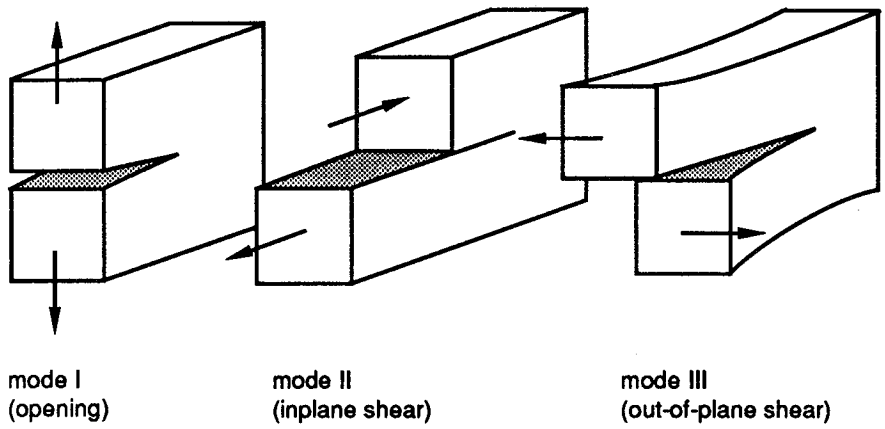

Figure 3. The three modes of crack–tip deformation.

2.2 Elastic Stress Field

Irwin's stress intensity approach is based on the elastic stress field near the crack tip. The stress components near the crack tip for mode I (Figure 4) have the form:

$$\begin{aligned}
\sigma_{xx} &= \frac{K_I}{\sqrt{2\pi r}} \cos\frac{\theta}{2}\left(1 - \sin\frac{\theta}{2}\sin\frac{3\theta}{2}\right), \\
\sigma_{yy} &= \frac{K_I}{\sqrt{2\pi r}} \cos\frac{\theta}{2}\left(1 + \sin\frac{\theta}{2}\sin\frac{3\theta}{2}\right), \\
\tau_{xy} &= \frac{K_I}{\sqrt{2\pi r}} \sin\frac{\theta}{2}\cos\frac{\theta}{2}\cos\frac{3\theta}{2}, \\
\tau_{xz} &= \tau_{yz} = 0, \\
\sigma_{zz} &= \begin{cases} 0 & \text{plane stress} \\ \nu(\sigma_{xx} + \sigma_{yy}) & \text{plane strain,} \end{cases}
\end{aligned}$$

where r is the distance from the crack tip, θ is the angle of inclination, and K_I is called the mode I stress intensity factor because its value governs the intensity of the stress field. [3]

Along the line ahead of the crack ($\theta = 0$):

$$\begin{aligned}
\sigma_{xx} &= \sigma_{yy} = \frac{K_I}{\sqrt{2\pi r}}, \\
\tau_{xy} &= 0.
\end{aligned} \tag{11}$$

The crack-tip stresses of equation 11 are proportional to $r^{-1/2}$, approaching infinity as r approaches zero. The stresses for all mode I problems have the form given by equation 11 regardless of boundary conditions and crack length. K_I changes its value to reflect differences in boundary conditions, relative crack length, and crack geometry.

The stress intensity factor is the basic parameter in LEFM because it controls the magnitude of the stress singularity of equation 11. For a given specimen shape, crack length, and the load, the stress intensity factor can usually be determined from a handbook. For example, the stress intensity factor for the large cracked plate shown in Figure 1 is:

$$K_I = \sigma\sqrt{\pi a}. \tag{12}$$

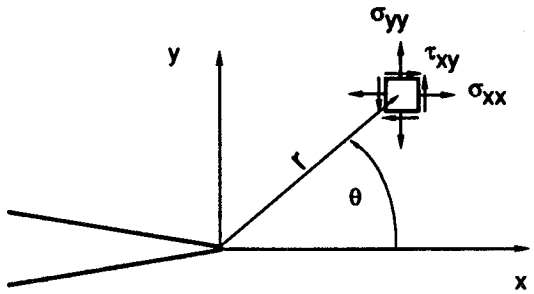

Figure 4. Crack–tip stresses for mode I.

Therefore, the stress intensity factor is proportional to the remote applied stress σ and the square root of length. K_I has the units of ksi$\sqrt{\text{in}}$ in the English system and MPa$\sqrt{\text{m}}$ in the SI system. Table 1 contains common conversion factors between the two systems of units. Modes II and III also have stress fields which exhibit the $r^{-1/2}$ singularity. Their stress fields are characterized by the stress intensity factors K_{II} and K_{III} and are defined similarly to K_I. [5]

For a given mode of crack–tip deformation, the total stress intensity factor can be determined using linear superposition — summing the stress intensity factors of all

Table 1. Conversions from English to SI units.

Quantity	English unit	× Conversion	= SI unit
Length	in	0.039	mm
Force	lb	4.448	N
Stress	ksi (10^3 psi)	6.895	MPa
Stress Intensity Factor	ksi$\sqrt{\text{in}}$	1.098	MPa$\sqrt{\text{m}}$
Temperature	°F	$\frac{5}{9}$(°F − 32)	C

loads acting to create that mode of deformation. Stress intensity factors from different modes cannot be summed: $K_{total} \neq K_I + K_{II} + K_{III}$. However, strain energy release rates can be summed regardless of the mode of deformation: $G_{total} = G_I + G_{II} + G_{III}$. Using the relationships between G and K for each mode leads to:

$$G_{total} = \frac{K_I^2}{E'} + \frac{K_{II}^2}{E'} + \frac{(1+\nu)\,K_{III}^2}{E}. \tag{13}$$

The relationship between K_I and a for most geometries is more complicated than the Griffith problem. In general, the stress intensity factor can be expressed:

$$K_I = \lambda \sigma \sqrt{\pi a}, \tag{14}$$

where λ [6] is the correction factor applied to the solution of the Griffith problem ($\lambda = 1$) in Figure 1. The factor λ depends on specimen geometry, relative crack length and shape, and loading.

2.3 Crack–Tip Plasticity

The mathematical stress field contains infinite stresses at the crack tip. Certainly, a real material cannot withstand infinite stresses. When the yield strength is exceeded near the crack tip, a limited amount of plastic flow occurs. Therefore, the theoretically infinite stresses are prevented by the presence of the crack–tip plastic zone shown in Figure 5. Plasticity makes the crack behave as if it were longer than its actual length because the crack–tip plastic zone results in larger crack–tip displacements and reduced local stiffness. Irwin estimated the first–order (elastic) size of the plastic zone by letting σ_{yy} in equation 11 equal the yield stress σ_{ys} and solving for the distance r_y. For thin plates (whose constraint is referred to as plane stress):

$$r_y = \frac{1}{2\pi}\left(\frac{K_I}{\sigma_{ys}}\right)^2. \tag{15}$$

For thick plates (whose constraint is referred to as plane strain), an additional component of stress, σ_{zz}, inhibits plastic flow, making the plastic zone smaller by a factor of three:

$$r_y = \frac{1}{6\pi}\left(\frac{K_I}{\sigma_{ys}}\right)^2. \tag{16}$$

[6] λ expressions for several geometries are given in section 3.4.

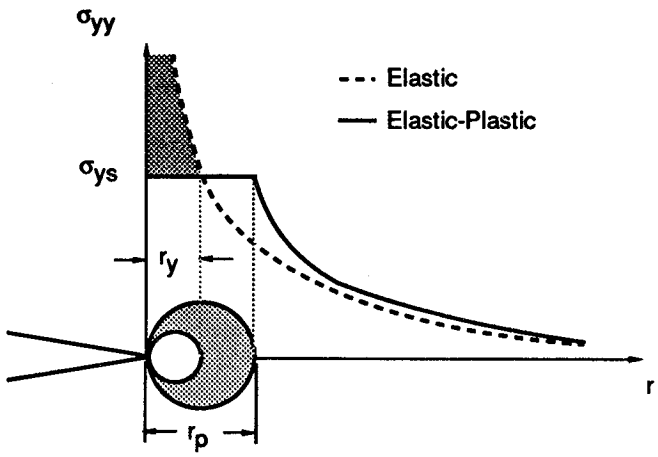

Figure 5. First–order and second–order approximations of plastic zone

Irwin estimated the second–order (elastic–plastic) size of the plastic zone r_p by redistributing the stresses from the crack tip to the first–order plastic zone:

$$\sigma_{ys}\, r_p = \int_0^{r_y} \sigma_{yy} dr, \tag{17}$$

which leads to the result:

$$r_p = \frac{1}{\pi}\left(\frac{K_I}{\sigma_{ys}}\right)^2 = 2\, r_y. \tag{18}$$

Irwin showed that the actual stress intensity factor was approximated by treating the crack as having length $a + r_y$. This approximation amounts to moving the crack tip to the center of the second–order plastic zone in Figure 5. Therefore, to apply the plastic zone correction consistently, the stress intensity factor should be corrected:

$$K_I = \lambda\sigma\sqrt{\pi(a + r_y)}. \tag{19}$$

where $a + r_y$ is the corrected crack length. The stress intensity factor can be rewritten to express the effect of the plastic zone:

$$K_I = \lambda\, \eta\, \sigma\sqrt{\pi a}, \tag{20}$$

where η is a factor representing the increase in stress intensity due to the existence of a plastic zone. η is a function of geometry, crack size, constraint, and ratio of stress–to–yield strength:

$$\eta = \frac{1}{\sqrt{1 - \frac{\lambda^2}{\alpha}\left(\frac{\sigma}{\sigma_{ys}}\right)^2}}, \tag{21}$$

where $\alpha = 2$ for plane stress and $\alpha = 6$ for plane strain. If the radicand in the denominator of the above equation becomes less than zero, plastic zone instability occurs. This condition represents the limit of applicability of LEFM for monotonic loading.

If K_I is expressed in a complicated manner, then η may be difficult to determine in closed form. In this case, iteration can be used to find the corrected K_I, starting with $K_I = \lambda\sigma\sqrt{\pi a}$ as the initial guess. Usually, only three or four iterations are required to achieve the desired convergence. A value for r_y can be calculated after K_I is corrected.

Understanding the mechanics of crack–tip plasticity is very important. A state of near–hydrostatic tension can exist at the crack tip; the tension is triaxial for plane strain constraint or biaxial for plane stress contraint on an infinitesimal element. The near–hydrostatic tension inhibits plastic flow which increases the tendency toward brittle behavior. In thick plates, constraint varies from a triaxial state of stress in the interior to a biaxial state of stress on the surface. A plate of intermediate thickness has a plane stress plastic zone on the surface and has a plastic zone approaching the condition of plane strain in the plate interior. Therefore, the dominant stress state is difficult to determine for a plate of intermediate thickness. To estimate whether the stress state is predominantly plane stress or plane strain, the following empirical rules can be used:

- Plane stress is expected if the calculated plane stress plastic zone size $2r_y$ is of the order of the plate thickness.
- Plane strain is expected if the calculated plane stress plastic zone size $2r_y$ is no larger than ten percent of the plate thickness. [4]

The following criteria may be used to determine if a plastic zone correction should be made:

$$\begin{array}{cl} \sigma \leq 0.5\sigma_{ys} & K_I = \lambda\sigma\sqrt{\pi a}, \\ 0.5\sigma_{ys} < \sigma \leq 0.85\sigma_{ys} & K_I = \lambda\sigma\sqrt{\pi(a + r_y)}, \\ 0.85\sigma_{ys} < \sigma & \text{elastic–plastic solution needed.} \end{array} \tag{22}$$

These criteria denote the limits of applicability of LEFM for monotonic loading. Detailed models of crack–tip plastic zones can be found in References [3]–[5].

3 STRESS INTENSITY FACTOR SOLUTIONS

3.1 Analytical Methods

The finite element method (FEM) is a very powerful analytical technique that can be used to determine crack tip displacements and stresses. Two simple approaches using FEM to determine stress intensity factors are the stress or displacement matching approach and the energy approach. In the stress matching approach, K_I is determined using extrapolated stresses or displacements (more accurate) near the crack tip. In the energy approach, K_I is computed using its relationship to strain energy release or compliance (inverse of stiffness).

For the stress matching approach, finite elements with a displacement function that includes a strain singularity of order $r^{-1/2}$ are used to model the crack tip. Directly ahead of the crack tip, K_I can be found using:

$$K_I = \lim_{r \to 0} \sigma_{yy} \sqrt{2\pi r}. \tag{23}$$

A plot of $\sigma_{yy}\sqrt{2\pi r}$ as a function of r is developed and K_I is extrapolated. A sample mesh is shown in Figure 6 and the extrapolation is shown in Figure 7. The extrapolation does not use stress and displacement data very near the crack tip because of the presence of the plastic zone. The major drawback of the stress matching method is that very small elements near the crack tip are required to obtain reasonable accuracy. [5]

Energy methods use relationship between K_I and G_I and the the definition of G_I:

$$G_I = \frac{K_I^2}{E} = \frac{dU}{da} \approx \frac{U_2 - U_1}{a_2 - a_1}. \tag{24}$$

where U_1 is the strain energy associated with a_1, and U_2 is the strain energy associated with $a_2 = a_1 + \delta a$. Two separate sets of solutions are needed to approximate the differential change in strain energy. As before, a fine mesh is required to develop the correct strain gradient. Alternatively, the compliance C (displacement divided by load) for a range of crack sizes can be determined. For a cracked body loaded by force P, the crack driving force G_I is:

$$G_I = \frac{P^2}{2t} \frac{dC}{da}. \tag{25}$$

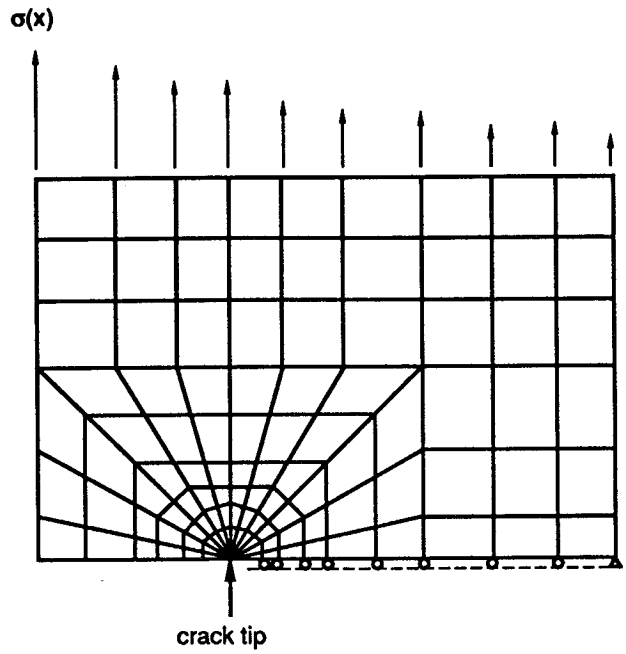

Figure 6. FEM mesh for an edge crack in a plate.

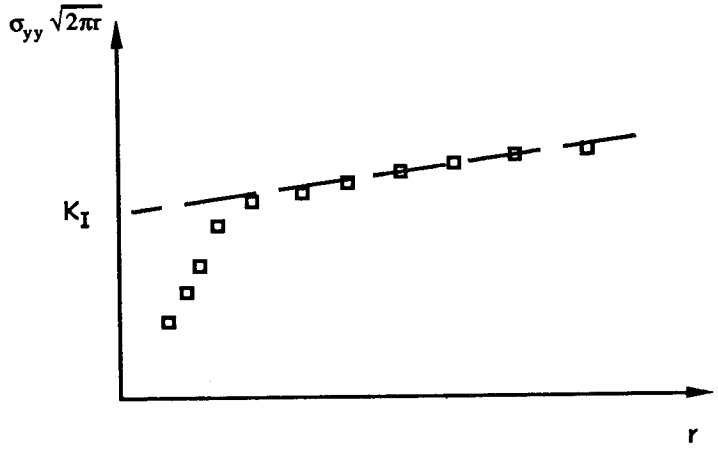

Figure 7. Extrapolating for K_I using stress matching method.

The stress intensity factor can then be determined using the relationship between G_I and K_I. [3, 5]

The use of FEM to solve fracture mechanics problems continues to be very active. References [19]–[21] provide an updated overview of FEM–based fracture mechanics and the special problems encountered when modeling cracks.

Another important method used to solve fracture mechanics problems is the boundary integral equation method (BIEM). Unlike FEM, BIEM does not require the meshing of the interior of a body. BIEM relies on the use of Betti's reciprocal theorem which relates work done on a body by two distinct loadings. BIEM can be a very efficient method for calculating stress intensity factors, but its use for nonlinear problems is more difficult. [5, 22]

3.2 Experimental Methods

The use of strain gages on actual hardware is a very powerful technique for determining stress intensity factors. First, strain gages measure ϵ_x and ϵ_y near the crack tip. Then the stresses are computed using:

$$\sigma_{xx} = \frac{E}{1-\nu^2}(\epsilon_x + \nu\epsilon_y),$$
$$\sigma_{yy} = \frac{E}{1-\nu^2}(\epsilon_y + \nu\epsilon_x).$$

The stress intensity factor is determined in the same manner as the FEM. Special care must be taken to avoid placing the gage within the plastic zone. Additionally, the size of the gage dictates that only rough estimates of stress intensity can be found. [3]

The experimental fatigue crack growth method [7] shown in Figure 8 is exceptionally useful for failure analysis. In many cases, the fracture surface reveals macroscopic lines or "beach marks" showing the location of the crack front at some point in time. Beach marks occur when there are significant interruptions or changes in fatigue loadings, such as the startup and shutdown of a turbine engine. The spacing between beach marks represents the crack growth per loading block (mission) or the average fatigue crack growth rate between significant changes in loading.

The fatigue crack growth rates, $\frac{da}{dN}$, of a complex configuration for which K_I is sought are compared with the fatigue crack growth rates of a standard test specimen

[7] A discussion of fatigue crack growth rates is given in section 5.

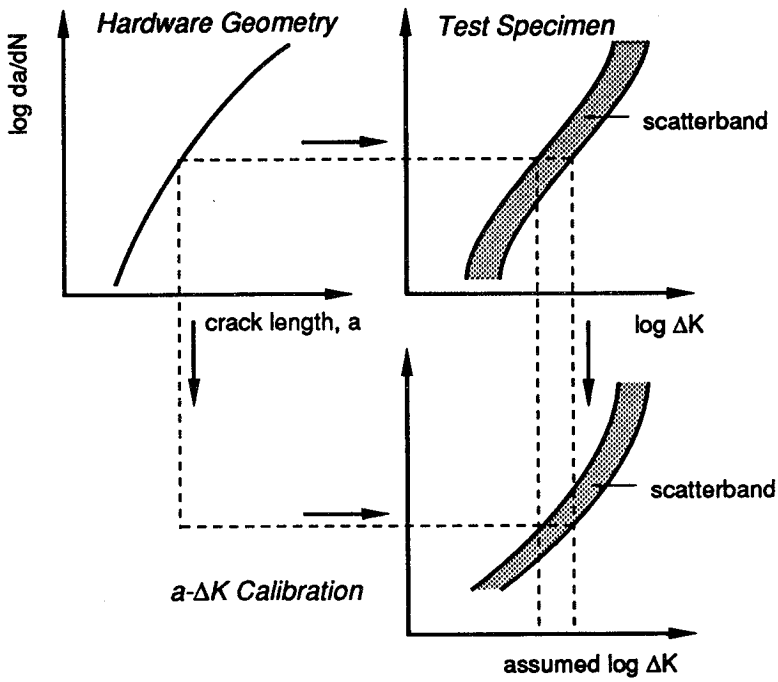

Figure 8. Experimental fatigue crack growth method.

of the same material. The experimentally measured crack lengths are correlated to the ΔK from a standard specimen for the same $\frac{da}{dN}$. For a through crack:

$$\Delta K = \Delta\sigma\, \lambda\sqrt{\pi a}, \tag{26}$$

where λ is the correction factor to be determined for the complex configuration. Although the crack growth rates for the complex geometry may have a scatterband, the method gives reasonable accuracy. [4]

3.3 Estimation Schemes

There are three widely used estimation schemes for stress intensity factors: superposition, compounding, and weight functions. The superposition principle states that the total stress intensity due to two or more different loads can be obtained by algebraically summing the stress intensity factors due to each individual load. This is valid only for combinations of the same mode of crack–tip deformation. For example, the solution for a through crack under internal pressure can be derived from the solution for a through crack remotely loaded in tension as shown in Figure 9.

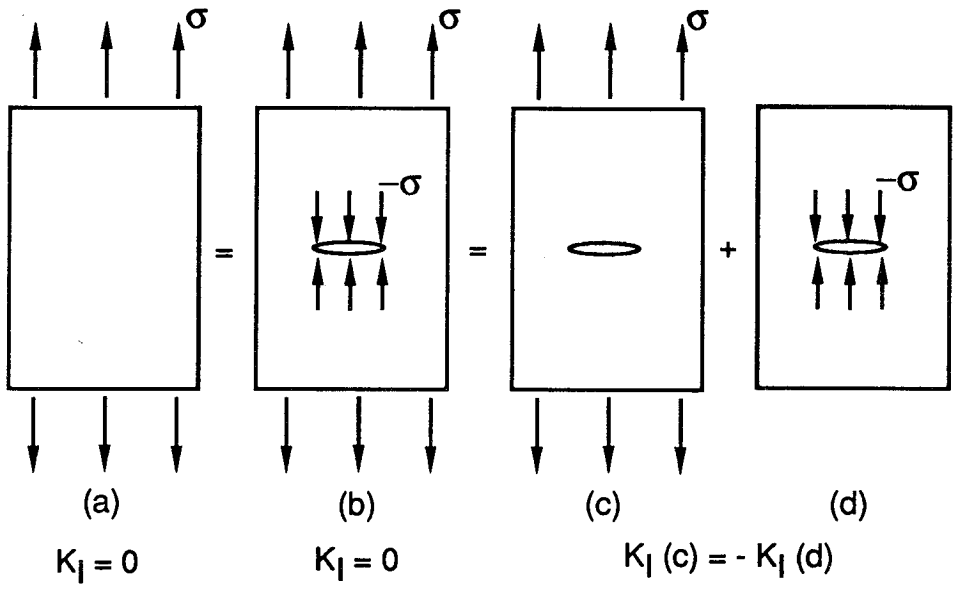

Figure 9. Superposition method.

In superposition, the stress intensity factors for the different load cases for a single geometry are summed. In the method of compounding, the same load case is used, but now information from the stress intensity factors for different geometries are used. Compounding can be used to account for boundary effects in solutions originally developed for finite plates as shown in Figure 10. The correction factor for two cracks growing out of a hole in a finite width plate is approximately equal to multiplying the correction factor for cracks growing out of a hole in an infinite plate by the correction factor for a crack in a finite width plate whose length is $D+2a$. [17]

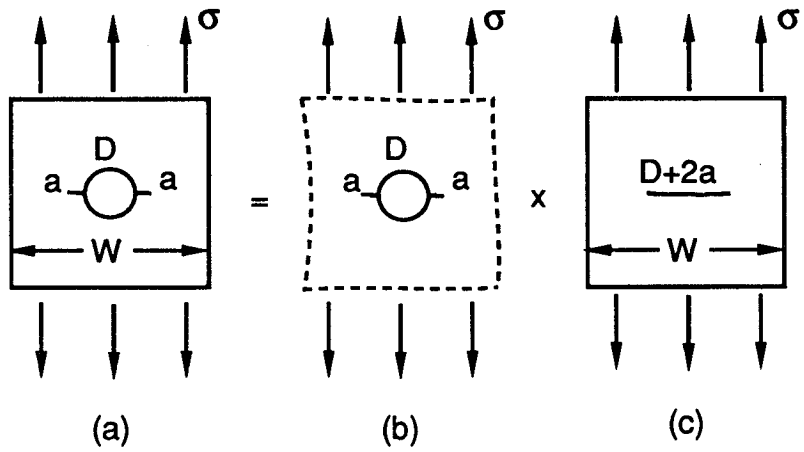

$$\lambda_{(a)} = \lambda_{(b)} \times \lambda_{(c)}$$

Figure 10. Compounding method.

The weight function method is based on superposition (Figure 9). The K_I for a through crack in a body with arbitrary remote loading is equal to the K_I for the same crack with a crack–face pressure distribution equal to the stresses calculated without the crack. This powerful method allows the stresses developed without consideration of the crack to be used to calculate the stress intensity factor. For example, the stress distribution from a FEM model that does not explicitly include a crack would be applied as crack–face pressures. In Figure 11a, the stress intensity factor for a point load on the crack face located at a distance b from the centerline of the crack is:

$$K_I(+a) = \frac{P}{\sqrt{\pi a}}\sqrt{\frac{a+b}{a-b}},$$

$$K_I(-a) = \frac{P}{\sqrt{\pi a}}\sqrt{\frac{a-b}{a+b}}.$$

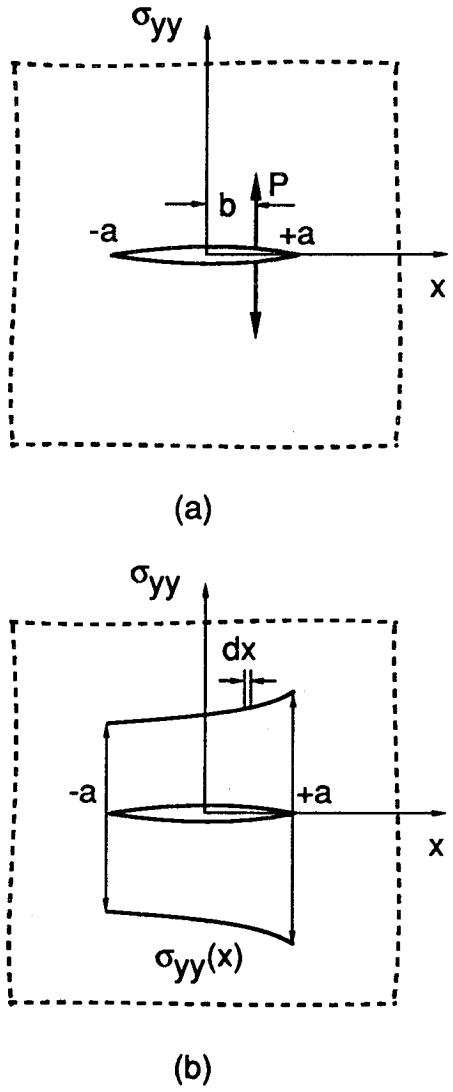

Figure 11. Weight function example.

At $b = 0$, the crack is loaded by a centrally located point force and the stress intensity factor is $K_I(\pm a) = P/\sqrt{\pi a}$. Therefore, if the load is constant, an increase in crack length causes a decrease in stress intensity factor.

The solution for a point load can be generalized now to find a solution for the arbitrary stress gradient on the crack faces shown in Figure 11b. The stress intensity factors are:

$$K_I(+a) = \frac{1}{\sqrt{\pi a}} \int_{-a}^{+a} \sigma(x) \sqrt{\frac{a+x}{a-x}}\, dx, \tag{27}$$

$$K_I(-a) = \frac{1}{\sqrt{\pi a}} \int_{-a}^{+a} \sigma(x) \sqrt{\frac{a-x}{a+x}}\, dx. \tag{28}$$

If $\sigma(x) = P$, then the above equations reduce to the case of uniform pressure on the crack faces: $K_I(\pm a) = P\sqrt{\pi a}$. [4]

For an uncracked stress field that can be approximated using a second–order polynomial, $\sigma = \sigma_{ref}(C_0 + C_1 x + C_2 x^2)$, the stress intensity factors for a through crack centered in an infinite plate are:

$$K_I(+a) = (C_0 + C_1 \frac{a}{2} + C_2 \frac{a^2}{2})\, \sigma_{ref} \sqrt{\pi a}, \tag{29}$$

$$K_I(-a) = (C_0 - C_1 \frac{a}{2} + C_2 \frac{a^2}{2})\, \sigma_{ref} \sqrt{\pi a}. \tag{30}$$

For higher-order polynomials, numerical integration should be used to determine K_I. Methods for obtaining stress intensity factor solutions using this method can be found in Reference [18].

3.4 K_I Solutions for Common Crack Geometries

3.4.1 Through Cracks

Recall the general expression for the stress intensity factor:

$$K_I = \lambda \sigma \sqrt{\pi a} \tag{31}$$

where λ is the crack geometry correction factor and σ is the remote stress. The following stress intensity factors were taken from References [24]–[27].

1. Center cracked plate ($\frac{a}{W} \leq 0.8$):

$$\alpha = \frac{a}{W}$$

$$\lambda = \sqrt{\sec\left(\frac{\pi a}{W}\right)}$$

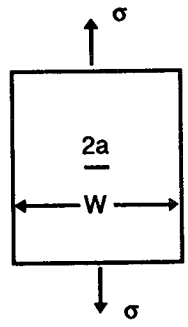

2. Edge cracked plate in tension ($\frac{a}{W} \leq 0.6$):

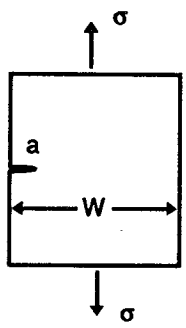

$$\begin{aligned} \alpha &= \frac{a}{W} \\ \lambda &= 1.122 - 0.231\alpha + 10.55\alpha^2 \\ &\quad -21.71\alpha^3 + 30.382\alpha^4 \end{aligned}$$

3. Edge cracked plate in bending ($\frac{a}{W} \leq 0.6$):

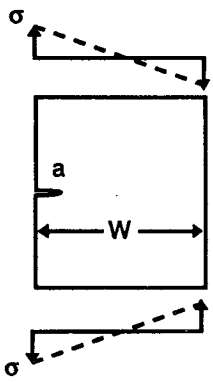

$$\begin{aligned} \alpha &= \frac{a}{W} \\ \lambda &= 1.122 - 1.4\alpha + 7.33\alpha^2 - 13.08\alpha^3 + 14.0\alpha^4 \\ \sigma &= \frac{6M}{W^2 t} \end{aligned}$$

4. Single crack at a hole in a plate under remote tension:

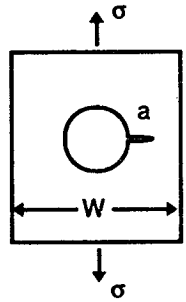

$$\begin{aligned} s &= \frac{a}{R+a} \\ \lambda &= [1 + 0.2(1-s) + 0.3(1-s)^6] \\ &\quad \times [2.243 - 2.64s + 1.352s^2 - 0.248s^3] \end{aligned}$$

5. Axial through crack in a thin-wall pressurized cylinder:

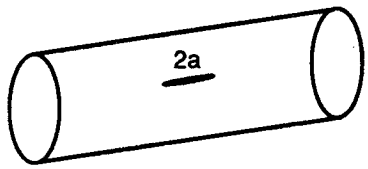

$$\begin{aligned} \lambda &= \sqrt{1 + 1.61\frac{a^2}{Rt}} \\ \sigma &= \frac{pR}{t} \end{aligned}$$

6. Compact tension specimen:

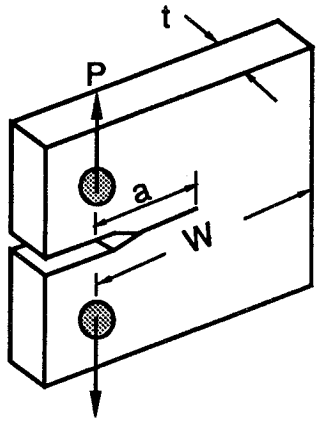

$$\begin{aligned}\alpha &= \frac{a}{W} \\ \lambda &= (0.886 + 4.64\alpha - 13.32\alpha^2 + 14.72\alpha^3 - 5.6\alpha^4) \\ &\quad \times (2+\alpha)/(1-\alpha)^{3/2} \\ \sigma &= \frac{P}{tW^{1/2}}.\end{aligned}$$

3.4.2 Elliptical Embedded and Surface Cracks

Actual cracks often initiate at surface discontinuities such as corners or internal discontinuities such as welds. To reduce the complexity of analyzing a crack in a three–dimensional body, the assumptions that the crack front remains in a plane and that the crack front remains elliptical are made. For relatively thick components, surface and corner cracks generally assume semi– or quarter–elliptical crack shapes as they grow under tension into the thickness. Similarly, embedded cracks generally assume elliptical shapes as they grow under tension. These observations are true as long as the crack is not close to geometric boundaries.

For an embedded elliptical crack in an infinite body, Irwin derived the expression:

$$K_I = \sigma \frac{\sqrt{\pi\, a}}{\Phi} \left(\sin^2 \phi + \frac{a^2}{c^2} \cos^2 \phi \right)^{1/4}, \tag{32}$$

where Φ is the elliptical integral of the second kind, and ϕ is the angle along the crack front shown in Figure 12. The elliptical integral is a function of a/c as given in Table 2.

K_I varies from a minimum of $\sigma\sqrt{\pi(a^2/c)}/\Phi$ at the ends of the major axis c ($\phi = 0$) to a maximum of $\sigma\sqrt{\pi a}/\Phi$ at the ends of the minor axis a ($\phi = \pi/2$). In the absence of free surfaces, an embedded elliptical crack loaded uniformly in tension will grow such that the aspect ratio a/c becomes circular ($a/c = 1$). For a circular crack, the stress intensity factor becomes:

$$K_I = \frac{2}{\pi} \sigma \sqrt{\pi a}. \tag{33}$$

For a surface crack, Irwin estimated that the presence of the front free surface of a semi–elliptical crack could be accounted for by compounding the correction factor for the embedded crack in an infinite body with the the correction factor for a small edge crack in a plate:

$$K_I = 1.12 \frac{2}{\pi} \sigma \sqrt{\pi a}. \tag{34}$$

If the crack intersects two front surfaces, such as a quarter–elliptical crack, then a correction factor of 1.2 should be used. If the surface or corner crack grows deeper than half the plate thickness, then a back surface correction factor must be used. This back surface correction is analogous to the correction factor for finite width effects for a through crack in a plate.

More accurate solutions based on finite element results for semi–elliptical cracks are given by J.C. Newman, Jr. and I.S. Raju. [28]–[30] Their solution for a flat plate loaded in tension and bending (Figure 13) is in the form:

$$K_I = (\lambda_w / \Phi) (\lambda_t \sigma_t + \lambda_b \sigma_b) \sqrt{\pi a}, \tag{35}$$

with λ_t given in Table 3, λ_b given in Table 4, and λ_w given by:

$$\lambda_w = \sqrt{\sec \left(\frac{\pi c}{W} \sqrt{\frac{a}{t}} \right)}. \tag{36}$$

Table 2. Elliptical integral of the second kind.

a/c	Φ	a/c	Φ
0.1	1.0160	0.6	1.2763
0.2	1.0505	0.7	1.3456
0.3	1.0965	0.8	1.4181
0.4	1.1507	0.9	1.4933
0.5	1.2111	1.0	1.5708

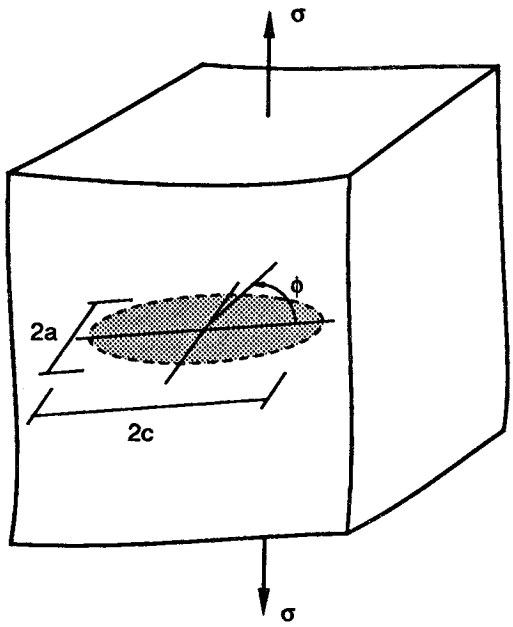

Figure 12. Embedded elliptical crack in an infinite body.

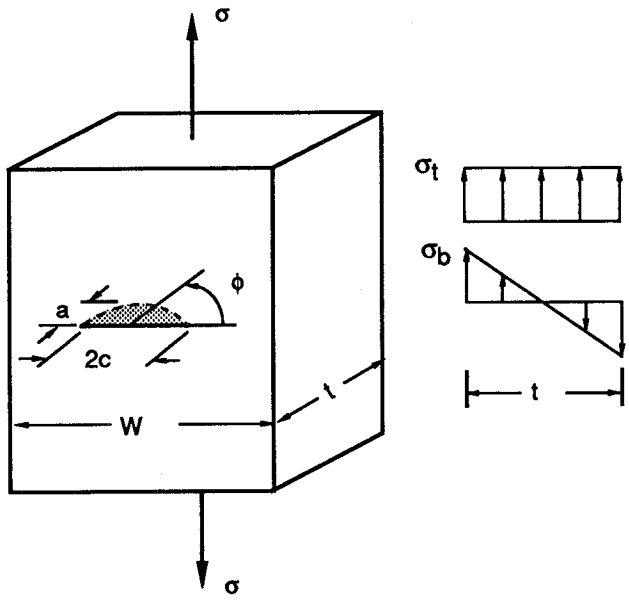

Figure 13. Surface crack in a plate.

Table 3. Surface crack tension correction factor (λ_t) by Newman and Raju.

		a/t			
a/c	ϕ	0.2	0.4	0.6	0.8
0.2	0	0.617	0.724	0.899	1.190
	$\pi/2$	1.173	1.359	1.642	1.851
0.4	0	0.767	0.896	1.080	1.318
	$\pi/2$	1.138	1.225	1.370	1.447
0.6	0	0.916	1.015	1.172	1.353
	$\pi/2$	1.110	1.145	1.230	1.264
1.0	0	1.174	1.229	1.355	1.464
	$\pi/2$	1.049	1.062	1.107	1.112

Table 4. Surface crack bending correction factor (λ_b) by Newman and Raju.

		a/t			
a/c	ϕ	0.2	0.4	0.6	0.8
0.2	0	0.572	0.629	0.701	0.787
	$\pi/2$	0.862	0.729	0.586	0.321
0.4	0	0.705	0.755	0.798	0.838
	$\pi/2$	0.830	0.629	0.416	0.123
0.6	0	0.838	0.851	0.862	0.868
	$\pi/2$	0.800	0.564	0.317	0.015
1.0	0	1.076	1.029	1.003	0.964
	$\pi/2$	0.742	0.482	0.207	-0.104

4 FRACTURE TOUGHNESS

4.1 Fracture Toughness Defined

Fracture toughness is defined as the material's critical stress intensity factor. While regarded as a material property, the fracture toughness of a given material may be strongly affected by operating temperature, heat treatment, and constraint (plate thickness). Therefore, care must be taken in design to use a value of fracture toughness which closely simulates the expected operating temperature and any corrosive environments present.

Constraint changes with plate thickness and strongly affects fracture toughness. Near the crack tip in thick plates, σ_{zz} develops normal to the plate surfaces. A state of triaxial tension (plane strain) exists in the material near the crack tip. The additional constraint inhibits plastic flow of material around the crack tip, promoting brittle behavior. In thinner plates, σ_{zz} exists to a lesser degree and more plastic flow occurs at the crack tip, dulling the crack tip and producing an apparent increase in fracture toughness. As plate thickness is increased, the critical stress intensity factor eventually approaches a lower bound as indicated in Figure 14. This lower bound value is called the plane strain fracture toughness, and the symbol K_{Ic} is reserved for this material property.

Operating temperature also strongly affects fracture toughness. As temperature decreases, the fracture toughness tends to decrease. For example, 4340 steel has a fracture toughness of 50 ksi$\sqrt{\text{in}}$ at $75°F$, but the toughness drops to 30 ksi$\sqrt{\text{in}}$ at $-100°F$. Therefore, fracture toughness is a material property that can vary considerably with temperature.

Fracture toughness can be used in the material selection process to screen candidate materials. One criterion for using fracture toughness that will ensure plane stress or high energy failure is:

$$K_{Ic} \geq \sigma_{ys}\sqrt{t}, \tag{37}$$

where t is the plate thickness. If this inequality can be achieved, then the design will be relatively insensitive to low energy failure due to crack–like defects. [4]

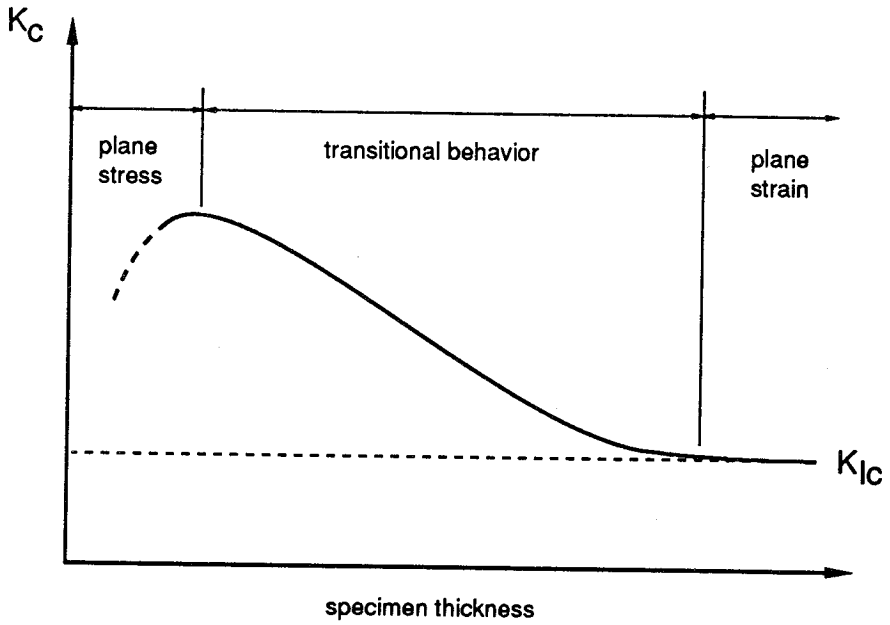

Figure 14. Dependence of fracture toughness on thickness.

The following literature references contain fracture toughness values for many high–strength materials used in aerospace applications:

- Damage Tolerant Design Handbook [31]
- Aerospace Structural Metals Handbook [32]
- Metallic Materials and Elements for Aerospace Vehicle Structures MIL–HDBK–5F [33]
- "A Compendium of Sources of Fracture Toughness and Fatigue Crack Growth Data for Metallic Alloys Parts I–IV." [34]–[37]

Table 5 gives some typical yield strength and plane strain fracture toughness values for several materials at room temperature. The appropriate value of fracture toughness to be used in a given design situation must be determined with a great deal of judgement because of the many variables influencing the fracture process. An excellent discussion of the problems involved in using fracture toughness data from the literature is given in reference [38].

Table 5. Typical yield strength and fracture toughness at room temperature.

Material	σ_{ys} ksi	K_{Ic} ksi$\sqrt{\text{in}}$
AL 7075–T76	68.0	25.0
AL 6061–T6	42.0	27.0
AL 2024–T851	54.0	22.0
AL 2219–T87	66.0	35.0
Steel D6AC	214.0	66.9
Steel AISI 4340	180.0	90.0
Steel AISI 304	66.0	100.0
Maraging Steel	250.0	76.0
Ti–6AL–4V	126.0	105.5
Inconel 718	160.0	90.0

4.2 Plane Strain Fracture Toughness Testing

The American Society for Testing and Materials (ASTM) has developed a standard test procedure for determining plane strain fracture toughness. [39] The compact tension (CT) specimen, shown in Figure 15, is the most commonly used specimen geometry. First, the test specimen is fatigue precracked. The chevron notch on the CT specimen is used as a crack starter because it yields a reasonably straight through crack front during fatigue precracking. After the test is completed, the length of the fatigue precrack is measured on each surface and at three points equally spaced through the thickness. Assuming that the rest of the test requirements are satisfied, the test is considered valid if the surface crack lengths are within 10 percent of a and the three interior measurements are within 5 percent of a, where a is the average crack length based on the three interior measurements.

The specimen size must be carefully chosen so that the dimensions are large compared to the plastic zone size and to ensure a state of plane strain. The test standard requires the minimum plate thickness, t, and crack length, a:

$$a, t \geq 2.5\left(\frac{K_{Ic}}{\sigma_{ys}}\right)^2. \tag{38}$$

Using the plane strain plastic zone size gives:

$$a, t \geq \frac{2.5}{1/6\pi} r_y \approx 50 r_y. \quad (39)$$

Unfortunately, equation 38 implies that K_{Ic} must be known before the test to ensure validity of the results! Therefore, K_{Ic} is often overestimated based on experience with similar materials. Also, the largest practical thickness for the specimen is used.

Once the specimen is sized and manufactured, it is precracked using a fatigue loading with $K_{max} < 0.6K_{Ic}$. After precracking to a specified length, the test specimen is loaded to fracture. The crack opening displacement (Figure 15) and specimen load are recorded during the test. The three types load versus displacement plots from K_{Ic} tests are shown in Figure 16. Type I is characterized by gradually increasing nonlinearity and Type II is characterized by sudden crack extension and arrest or "pop–in" followed by nonlinearity. Type III is characterized by almost perfectly elastic behavior and is uncommon.

A candidate value of fracture toughness, K_Q, is calculated using the load P_Q determined as follows:

- The load corresponding to the intersection of a 5 percent secant offset line drawn from the origin with the load–displacement curve is denoted P_5.
- If the load–displacement plot is Type I, then $P_Q = P_5$.
- If the load–displacement plot is Type II, then P_Q is the highest load preceding P_5 on the load–displacement curve.
- If the load–displacement plot is Type III, then $P_Q = P_{max}$.

The ratio P_{max}/P_Q must be less than 1.1 to ensure that excessive stable crack growth does not occur during the test. The value of K_Q is calculated using the stress intensity factor equation from section 3.4. If all the previous conditions are met, the test is valid and $K_{Ic} = K_Q$. [4, 39]

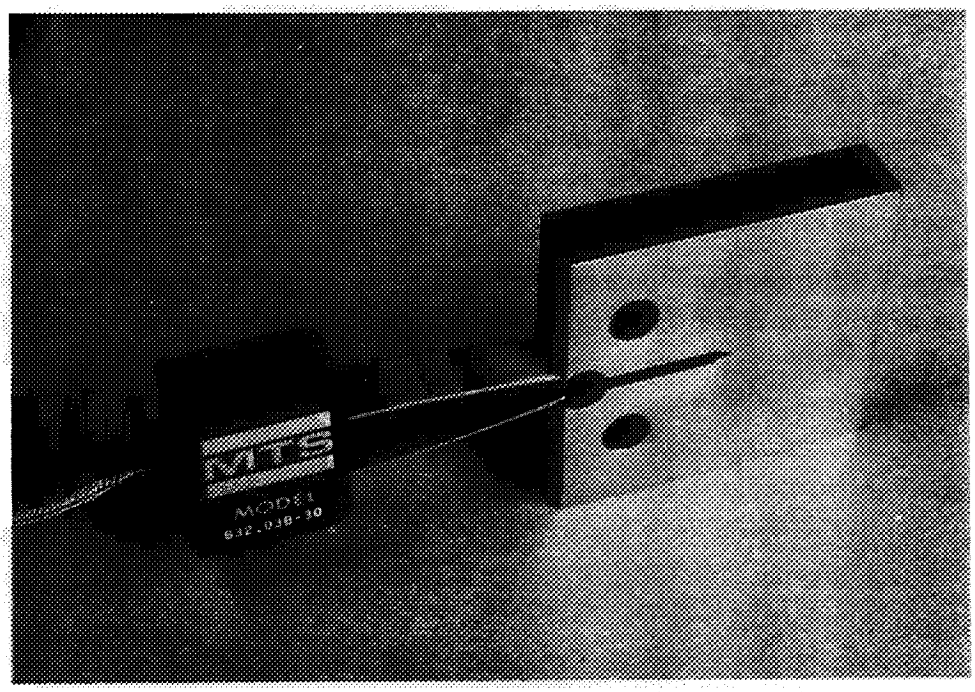

Figure 15. Compact tension fracture toughness specimen.

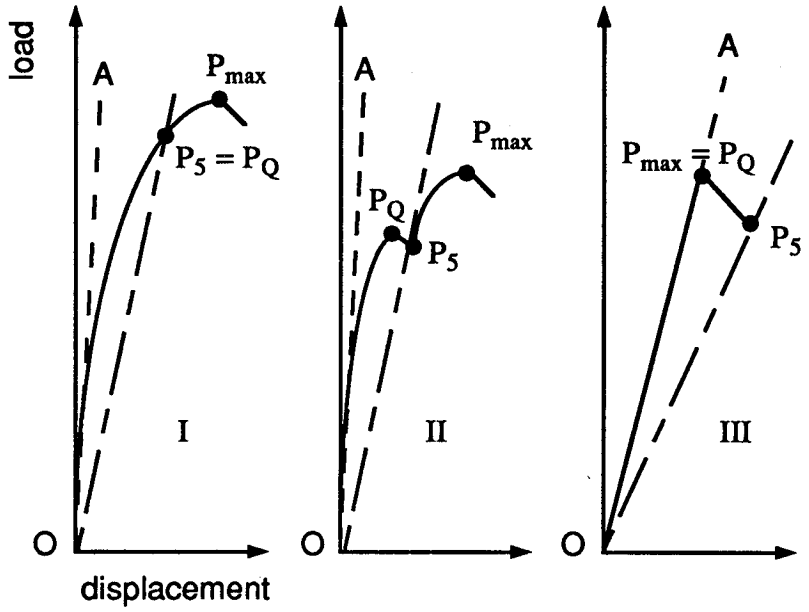

Figure 16. Types of load versus displacement plots from K_{Ic} tests.

4.3 Plane Stress Fracture Toughness Testing

Values of critical stress intensity factors for thinner plates are denoted simply as K_c, the plane stress or transitional fracture toughness. The thicknesses used in actual structures are often much less than the thickness needed for a valid K_{Ic} test. Therefore, a test–verified methodology for determining K_c is of practical interest.

The Feddersen approach considers a center crack, $2a_0$, in a thin plate loaded in tension. As shown in Figure 17, the crack will begin to grow stably during loading at an initial stress σ_0. Stable crack growth continues until the critical crack length $2a_c$ is reached at a stress σ_c, where the crack becomes unstable and fracture occurs. For a longer initial crack, stable crack growth begins at a lower initial stress level. More stable crack growth will occur for the longer initial crack; however, the critical stress is lower than for the smaller initial crack. K_c is the critical stress intensity factor for unstable crack growth (fracture) or plane stress fracture toughness:

$$K_c = \sigma_c \sqrt{\pi a_c}. \tag{40}$$

K_c is approximately constant for a given thickness and a small range of crack sizes.

The residual strength in terms of the initial flaw size can be found by relating the initial flaw size to the critical stress using the "apparent fracture toughness, " K_{c0}:

$$K_{c0} = \sigma_c \sqrt{\pi a_0}. \tag{41}$$

If the amount of stable crack growth is small, then $2a_0 \approx 2a_c$ and $K_{c0} \approx K_c$. Rewriting equation 41 leads to: $\sigma_c = K_{c0}/\sqrt{\pi a_0}$. Although $\sigma_c \rightarrow \infty$ as $2a_0 \rightarrow 0$, the residual strength cannot actually be larger than the yield strength. Additionally, as $2a_0 \rightarrow W$, $\sigma_c \rightarrow 0$. These observations lead to the conclusion that net section yielding occurs at the two extremes of crack length in the plate.

An estimate of the residual strength as a function of crack size can be made if two tangent lines are drawn to the critical stress curve. As shown in Figure 18, one tangent line connects the point $(2a_0 = 0, \sigma = \sigma_{ys})$ to the critical stress curve at the point where $\sigma = 2/3\ \sigma_{ys}$. The other tangent line connects the point $(2a_0 = W, \sigma = 0)$ to the curve at $2a_0 = W/3$. Experimental data support the use of these tangents and the critical stress curve between them for defining residual strength. Therefore, the requirements for a valid plane stress fracture toughness test are:

$$\sigma_c < \frac{2}{3}\sigma_{ys} \text{ and } 2a_0 < \frac{W}{3}. \tag{42}$$

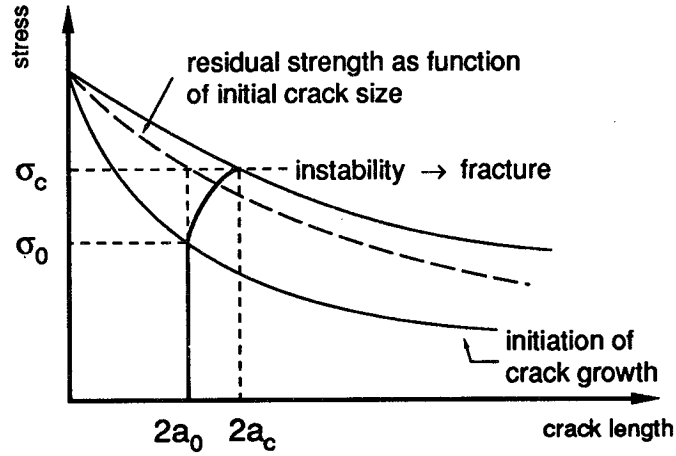

Figure 17. Growth of a through crack in a thin plate.

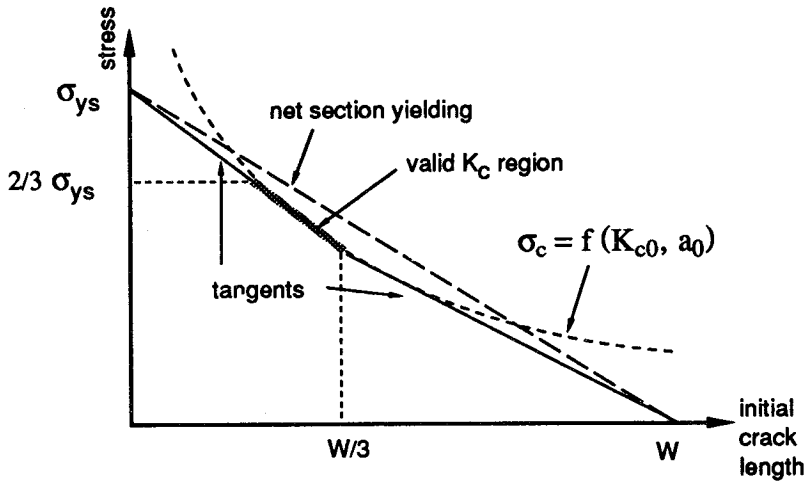

Figure 18. Engineering estimate of residual strength.

The K_c tests should be conducted on fatigue precracked specimens using the actual thicknesses and crack lengths of interest. Any stable crack growth during the test should be recorded, as well as the load and time. The fracture load should be taken as the maximum load in the test. Unconservative errors in estimating residual strength will result if the requirements on stress level and crack size are not met. [4]

5 SUBCRITICAL CRACK GROWTH

5.1 Fatigue Crack Growth

Fatigue cracks originate at geometric stress concentrations (holes and fillets) and at manufacturing flaws (tool scratches, impact dents, and pits caused by welding arc strikes). A fatigue crack can grow under the cyclic loading shown in Figure 19, finally reaching its critical length and fracturing. The stress range $\Delta\sigma = \sigma_{max} - \sigma_{min}$ can be related to the stress intensity factor range, ΔK:

$$\begin{aligned} \Delta K &= K_{max} - K_{min}, \\ \Delta K &= \lambda\sigma_{max}\sqrt{\pi a} - \lambda\sigma_{min}\sqrt{\pi a}, \\ \Delta K &= \lambda\Delta\sigma\sqrt{\pi a}, \end{aligned} \tag{43}$$

where K_{max} and K_{min} are the stress intensity factors associated with the maximum and minimum stresses in a fatigue cycle and λ is the correction factor discussed in section 3. The growth rate of a fatigue crack is related to ΔK and the load ratio, R:

$$R = \frac{K_{min}}{K_{max}}. \tag{44}$$

The fatigue crack growth rate, $\frac{da}{dN}$, is the crack extension Δa during a small number of fatigue cycles ΔN. Fatigue crack growth rate is a function of the stress intensity factor range ΔK and stress ratio R. Data of $\frac{da}{dN}$–ΔK for a given R are usually presented on a log–log plot as shown in Figure 20. The crack growth rate curve has a sigmoidal shape which divides the curve into three regions. In region I, a threshold value of ΔK occurs. Ideally, the crack will not grow if ΔK drops below this threshold. [8] Above ΔK_{th}, the crack growth rate increases rapidly with increasing ΔK. Crack growth rate in this region is influenced by microstructure, mean stress, and environment. Region II is characterized by a linear log–log relationship between $\frac{da}{dN}$ and ΔK; this region is influenced largely by certain combinations of environment, mean stress, and frequency. Microstructure and thickness have little influence on the crack growth of region II. In region III, the crack growth rate rises to an infinite slope caused when $K_{max} \rightarrow K_c$. Microstructure, mean stress, and thickness are large influences on the crack growth rate in this region. [3]

[8] ASTM has defined the stress intensity factor range threshold ΔK_{th} as the ΔK value associated with $\frac{da}{dN} = 4 \times 10^{-9}$ inches/cycle. [40]

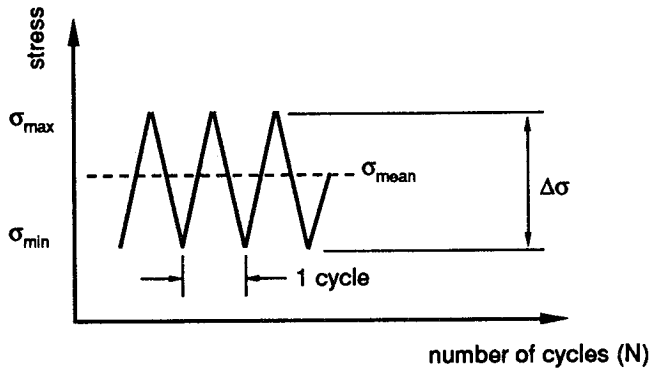

Figure 19. Stress–cycle parameters in constant amplitude fatigue.

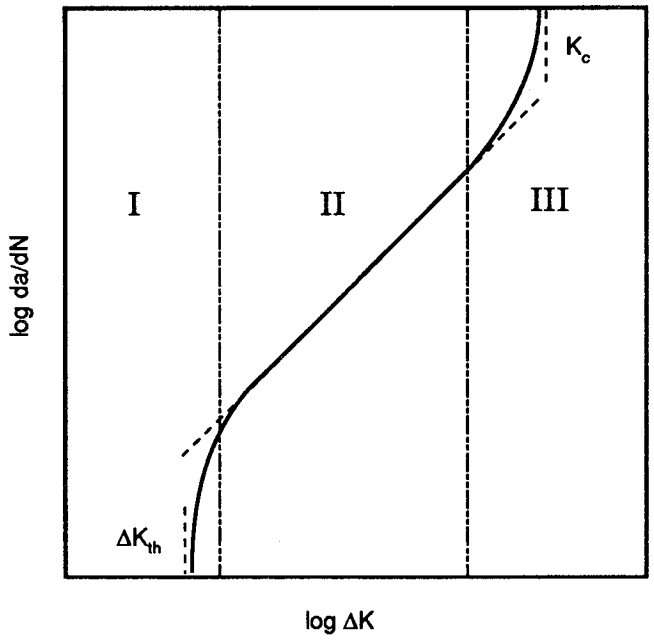

Figure 20. Fatigue crack growth rate as a function of ΔK.

As previously mentioned, a threshold value, ΔK_{th}, exists below which significant crack growth does not occur. Knowledge of ΔK_{th} has considerable practical advantage. If either sufficiently small flaws can be ensured by the planned inspection techniques or if sufficiently small working stresses are maintained such that ΔK is less than ΔK_{th}, then no fatigue crack growth can occur and the crack can never reach critical length. In some situations it may be desirable to design for nonpropagating flaws. However, threshold testing is very difficult to perform and the uncertainties involved in the analysis make design using $\Delta K < \Delta K_{th}$ questionable. The design problem of using $\Delta K < \Delta K_{th}$ is analogous to the problem of using $\Delta\sigma < \Delta\sigma_e$, where $\Delta\sigma_e$ is the fatigue endurance limit. Many materials have no true endurance limit and the stress range corresponding to a life of 10^8 cycles is used in place of $\Delta\sigma_e$. The use of arbitrary definitions for ΔK_{th} and $\Delta\sigma_e$ for an infinite life design should be viewed with skepticism.

Attempts to describe the crack growth rate curve using empirical formulas have been widespread. For a fixed load ratio, R, and a wide range of ΔK values in region II, the data can usually be represented as a straight line on the log–log plot. The Paris equation describes crack growth in region II:

$$\frac{da}{dN} = C(\Delta K)^n, \tag{45}$$

where C and n are empirical constants determined experimentally for the given material. The effects of load frequency, temperature, and operating environment are empirically contained in the constants C and n. Table 6 contains a list of these constants for different materials. Note that C has the units of in/cycle(ksi$\sqrt{\text{in}}$)$^{\text{n}}$ and n is a dimensionless exponent which can be thought of as the slope of the crack growth rate curve. Other dimensional units may be used, so care must be taken to maintain consistent units when peforming fatigue crack growth analysis. For most materials, the value of n ranges from 2 to 4.

The references listed in Section 4.1 for fracture toughness data also contain fatigue crack growth data. Special care should be taken if data from literature sources are used to ensure that the data correspond to the actual environment or are conservative with respect to the actual environment. Most $\frac{da}{dN}$–ΔK curves are generated using $R \approx 0$ and room temperature. For some materials, $\frac{da}{dN}$–ΔK curves have been generated at several different stress ratio, temperature and environments, and load frequency. Interpolation of these curves is often necessary and should be performed by experienced metallurgists and engineers. Guidelines for using literature sources are discussed in Reference [41].

Table 6. Typical Paris equation constants for room temperature and $R = 0$.

Material	C in/cycle(ksi$\sqrt{\text{in}}$)^n	n
AL 7075–T76	0.679×10^{-9}	3.250
AL 6061–T6	1.760	2.967
AL 2024–T851	3.090	4.745
AL 2219–T87	0.109	3.709
Steel D6AC	0.004	3.583
Steel AISI 4340	0.003	3.680
Steel AISI 321	0.181	2.775
Maraging Steel	2.030	2.098
Ti–6AL–4V	0.184	3.237
Inconel 718	0.109	2.707

The answer to the question of how to deal with reversed fatigue loading ($R < 0$) can be confusing. For example, an estimate of $\frac{da}{dN}$–ΔK for $R = -1$ ($K_{min} = -K_{max}$) can be made using $\frac{da}{dN}$–ΔK for $R = 0$. For $R = -1$, the stress intensity factor range is:

$$\Delta K = K_{max} - (-K_{max}) = 2K_{max}. \tag{46}$$

If a $\frac{da}{dN}$–ΔK curve for $R = 0$ is to be used in place of a curve for $R = -1$, then the ΔK used in the analysis should include only the positive part of the fatigue cycle for consistency with the curve used:

$$\Delta K = K_{max} - 0 = K_{max}. \tag{47}$$

Using equation 46 gives $\Delta K = 2K_{max}$ and equation 47 gives $\Delta K = K_{max}$. The factor of 2 difference in ΔK can be seen in Figure 21. Care should be taken when performing analysis for negative stress ratios to determine which definition for ΔK should be used.

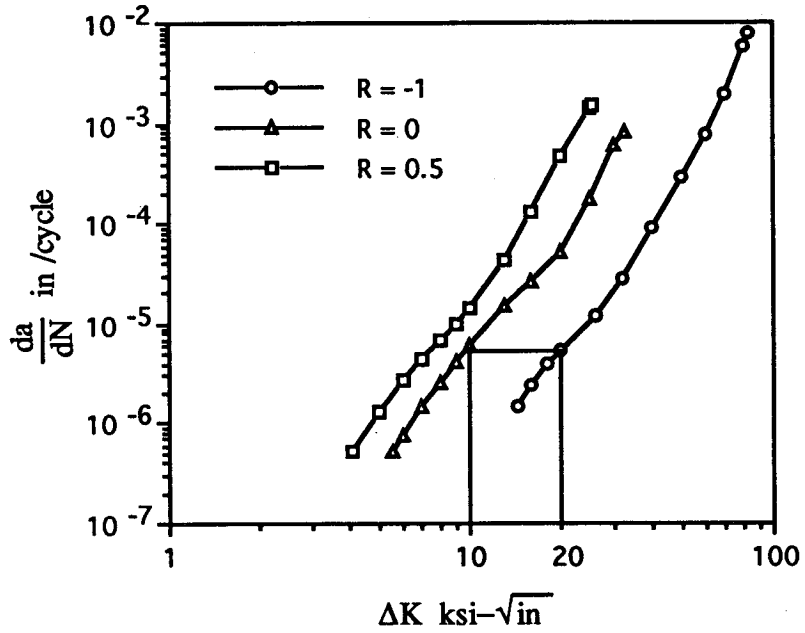

Figure 21. $\frac{da}{dN}$–ΔK for 7075–T6 aluminum alloy at room temperature.

The Forman equation allows the value of $\frac{da}{dN}$ to approach infinity as the maximum stress intensity factor in a fatigue cycle, as K_{max} approaches K_c. This behavior can be described as follows:

$$\frac{da}{dN} = \frac{C(\Delta K)^n}{(1-R)K_c - \Delta K}. \tag{48}$$

By taking K_{max} into account, the Forman equation describes regions *II* and *III*. The Walker equation accounts for the relatively weak influence of mean stress level on crack growth rate:

$$\frac{da}{dN} = C\left[\frac{\Delta K}{(1-R)^{1-m}}\right]^n. \tag{49}$$

The constants C and n in Paris, Forman, and Walker equations are not generally interchangeable: $C_{Paris} \neq C_{Forman} \neq C_{Walker}$ and $n_{Paris} \neq n_{Forman} \neq n_{Walker}$.

The hyperbolic sine equation is capable of fitting the entire crack growth rate curve:

$$\log \frac{da}{dN} = C_1 \sinh\left[C_2(\log \Delta K + C_3)\right] + C_4, \tag{50}$$

where C_1 is a material constant, and C_2, C_3, and C_4 can be written as functions of temperature, frequency, and stress ratio. This model [42] has been used extensively for nickel–base superalloys. Many other empirical equations have been used to describe fatigue crack growth. [3]–[5]

The equation used to express fatigue crack growth rate as a function of ΔK can be integrated to determine the number of cycles required for the crack to reach a given length. For example, the Paris equation (equation 45) can be used to determine the number of cycles to failure. To perform the integration, ΔK must be expressed in terms of the crack length, a. If a_i and a_f are initial and final crack lengths, N_f is the number of cycles required for the crack to reach a length of a_f is:

$$N_f = \int_0^{N_f} dN = \int_{a_i}^{a_f} \frac{da}{C(\Delta K)^n}. \tag{51}$$

If the stress spectrum is known, then the final crack size can be determined as follows:

$$a_f = a_i + \int_1^{N_f} C(\Delta K)^n dN \approx a_i + \sum_{j=1}^{N_f} C(\Delta K_j)^n, \tag{52}$$

where ΔK_j is a function of Δa_j.

In the discussion on crack–tip plastic zones, the approach was to determine a correction factor, r_y, for the crack length to account for increased compliance due to the presence of the plastic zone for steady, monotonic loading. For fatigue loading, the material must accommodate the deformed region, and reversed yielding occurs in a region smaller than the monotonic plastic zone. The cyclic plastic zone is smaller than the monotonic zone because the crack extends into this smaller zone of reversed yielding:

$$r_{y,cyclic} = \frac{r_{y,monotonic}}{4}, \tag{53}$$

where $r_{y,monotonic}$ is defined in section 2.3. [5]

Even under general monotonic yielding, LEFM may be valid for fatigue crack growth because crack growth depends on the cyclic variation of strain instead of the maximum crack–tip strain. If the crack length and remaining ligament are greater than the cyclic plastic zone size, then using ΔK as the crack driving force should be acceptable. Therefore, the limit of applicability of LEFM for cyclic crack growth is not as restrictive as the limit for monotonic crack growth. [43, 44]

Another important limitation of LEFM fatigue crack growth is the physical size of the crack. Cracks less than 0.04 in long are referred to as "short cracks," and are much smaller than the crack sizes normally used in generating fatigue crack growth rate curves. Similitude between fatigue crack growth rate and stress intensity factor range is lost because short cracks tend to grow at higher rates than expected from $\frac{da}{dN}$–ΔK data taken from long cracks.[3, 5]

The previous discussions on fatigue crack growth dealt with the use of fatigue crack growth rates determined from constant amplitude cyclic loading tests. These crack growth rates are approximately the same as for random cyclic loading tests if the maximum stress is held constant and the mean stress and stress range vary randomly. In the case of variable amplitude loading where maximum stress is also allowed to vary, the sequence or order of loading cycles can have a significant effect on crack growth rate. The result is that overall crack growth for random load cycles can be substantially higher than for constant amplitude load cycles.

Fatigue damage and crack growth are dependent on previous cyclic load history. A significant delay in crack growth can occur after the intermittent application of high stresses. This delay is called retardation and can be characterized as a period of reduced crack growth rate following the application of a peak load higher and in the same direction as the peak loads immediately following. Acceleration can be characterized as a period of increased crack growth due to the application of

a crack closing overload cycle. Crack growth calculations which account for both retardation and acceleration can dramatically improve the accuracy of fatigue crack growth predictions. [3, 6, 23]

5.2 Sustained Load Crack Growth

Sustained load crack growth is time–dependent subcritical crack growth occuring under a stress well below tensile failure. Examples of sustained load crack growth are creep crack growth, stress corrosion cracking, and hydrogen embrittlement. Creep crack growth usually occurs at temperatures greater than fifty percent of the melting point. Creep crack growth is a very important problem in the power industry and in aircraft gas turbine engines. The reader should consult References [45, 46] for more details about creep cracking.

Stress corrosion cracking occurs when a crack grows at a given sustained stress intensity level. This mechanism of crack growth is particularly important when dealing with pressure vessels which must maintain significant loads for long time periods. As shown in Figure 22, the crack growth rate da/dt can be correlated with stress intensity K_I much in the same way that fatigue crack growth rate da/dN can be correlated with the stress intensity range ΔK. K_I is used to describe stress corrosion cracking for test specimens with the thickness range and environment of interest to the designer. A threshold stress intensity for stress corrosion cracking K_{Iscc} can be determined experimentally; however, K_{Iscc} should not be generally considered a material property because the testing time required to establish a true threshold for crack growth may be much longer than the actual testing time. Additionally, the sensitivity of K_{Iscc} to service environment should be examined when using data from the literature. [4]

Hydrogen embrittlement cracking can occur when a susceptible material is exposed internally or externally to gaseous hydrogen. Hydrogen diffuses into many steels and Ni–base and Ti–base alloys. The effects of hydrogen embrittlement can be expressed in terms of $da/dt - K_{max}$ in the same manner as stress corrosion cracking. Alternatively, the effects of hydrogen embrittlement can be implicitly expressed in fatigue crack growth rate data da/dN–ΔK if hold times are programmed into the load cycles.

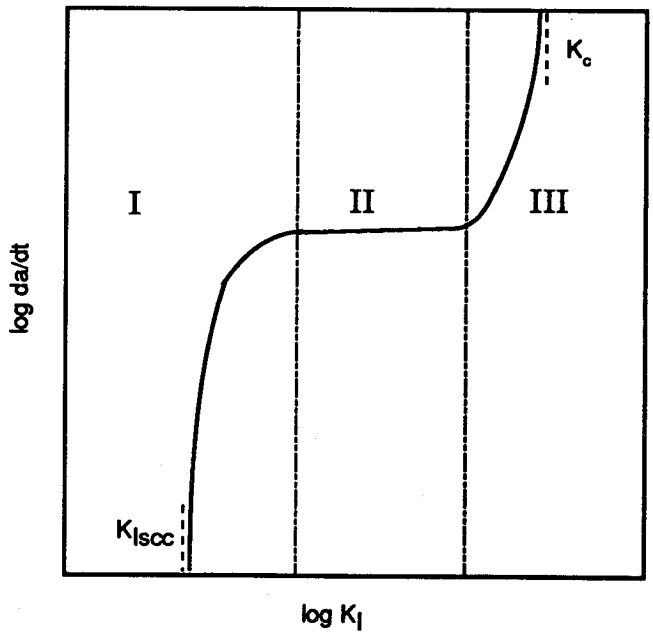

Figure 22. Sustained load crack growth rate as a function of K_I.

6 DAMAGE TOLERANCE AND FRACTURE CONTROL

6.1 Philosophy and Basic Assumptions

Damage tolerance and fracture control are both terms used to describe the rigorous application of engineering, manufacturing, quality assurance, and operations dealing with the analysis and prevention of crack growth or similar flaw damage leading to catastrophic event. A catastrophic event is usually defined as a failure event causing loss of life, injury, or the loss of spacecraft. Fracture control is applied to ensure safety; fracture control is not mandatory to ensure mission success. However, fracture control principles should be considered in design even when safety is not an issue.

The general goals of fracture control include the selection of fracture resistant materials and manufacturing processes, designing access for inspectability, and the use of multiple load paths or crack stoppers. These goals translate into two specific objectives: design for safe, stable crack growth (safe–life design) or design for damage containment due to structural redundancy (fail–safe design). Fracture control requires the judicious combination of safe–life and fail–safe design. Careful stress analysis, geometry selection, material selection, surface finish, and workmanship are necessary prerequisites to effective fracture control.

MSFC–HDBK–1453, "Fracture Control Program Requirements," [51] specifies that the fracture control status of all spaceflight structures must be determined. If a structural failure of a part would cause a catastrophic event, then the part is fracture sensitive. MSFC–HDBK–1453 divides the previously defined fail-safe class into three subclasses:

- Low mass parts whose release or functional loss will not cause a catastrophic event
- Contained or restrained parts whose structural failure will not cause a catastrophic event
- Structurally redundant (called fail–safe in MSFC–HDBK–1453) parts whose remaining structure will not cause a catastrophic event.

If a fracture sensitive part cannot be classified as low mass, contained, or fail–safe, the part is fracture critical. All pressure vessels and high–energy rotating machinery are classified as fracture critical. A fracture critical part must have a safe–life design; it must survive 4 complete mission lifetimes in the presence of the largest possible

undetected flaw. MSFC–HDBK–1453 specifically uses safe–life to describe metallic or glass components and damage-tolerant to describe composite components. Fracture mechanics analyses or tests, flaw screening, and general traceability to ensure proper implementation and documentation of the fracture control process are required for fracture critical parts. MSFC-SPEC-522B, "Design Criteria for Controlling Stress Corrosion Cracking," [47] should be used as a guide in selecting materials to avoid stress corrosion cracking problems.

There are four basic assumptions for safe–life design:

1. Crack–like flaws are inherent in new structures and exist in the most critical location and orientation.

2. Similitude exists between test specimens and actual hardware so that fracture toughness and fatigue crack growth rate data obtained from test specimens can be used to predict fatigue crack growth and final crack instability in actual flight hardware.

3. It is assumed that a scatter factor (the scatter factor in MSFC–HDBK–1453 is 4) can be applied to the service life to conservatively account for scatter in fracture mechanics material properties and uncertainties in analyses due to using constant amplitude fatigue crack growth data to analyze parts undergoing variable amplitude loading.

4. It is assumed that adequate flaw screening (nondestructive inspection or proof testing) can be reliably performed on fracture critical parts.

The proper way to implement these fracture control requirements is to develop a fracture control plan. The fracture control plan documents the design, materials, fabrication, inspection, and operation activities used to prevent catastrophic failures due to cracks. C.C. Osgood [48] has written an outline for a fracture control plan of a high–performance engineering system:

Design

1. Determine stress and strain distributions.
2. Determine flaw tolerance for regions of greatest fracture hazard.
3. Estimate stable crack growth for typical service periods.
4. Recommend safe operating conditions and specify intervals between inspections.

Materials

1. Determine yield and ultimate strengths.
2. Determine fracture parameters: K_c, K_{Ic}, K_{Iscc}, da/dN.
3. Establish recommended heat treatments.
4. Establish recommended welding methods.

Fabrication

1. Control residual stress, grain growth, and grain direction.
2. Develop or protect strength and fracture properties.
3. Maintain fabrication records.

Inspection

1. Inspect part prior to final fabrication.
2. Inspect fabrication factors such as welding current and speed.
3. Proof test.
4. Estimate largest crack–like defect sizes.

Operation

1. Control stress level and stress fluctuations in service.
2. Protect part from corrosion.
3. Inspect part periodically.

6.2 Flaw–Screening Methods

6.2.1 Nondestructive Inspection

Critical initial flaw sizes are calculated for all likely crack locations in the structure using fracture mechanics, then nondestructive inspection (NDI) [9] is used to reliably find flaws at those locations. MSFC–STD–1249, "Standard NDE Guidelines and Requirements for Fracture Control Programs" [49] requires that the smallest flaw that NDI can reliably detect must be smaller than critical initial flaw size. Table 7 contains a list of approved initial flaw sizes for several NDI methods. Initial flaws smaller than those shown in Table 7 may be assumed if a NDI demonstration verifies that a 90 percent probability of detection with a 95 percent confidence level exist for the smaller size.

[9] Nondestructive inspection (NDI) is also called nondestructive testing (NDT) or nondestructive evaluation (NDE).

A. P. Parker [50] describes the common NDI methods:

- *Eddy current.* A small coil induces eddy currents in the metal component. This reinduces a current in the coil. A change in the inductive "fingerprint" of a component may indicate a crack or defect.
- *Dye-penetrant.* Suitable for surface cracks only, the method involves the application of a liquid penetrant, which is subsequently wiped off the surface before application of a powdered "developer." Cracklike defects will produce a contrasting colored line on the developer.
- *Magnetic particles.* Fluorescent liquid containing iron particles in suspension is applied to a component. When placed in a strong magneteic field and illuminated with ultraviolet light, disturbances in magnetic field induced by cracks and cutouts appear as a change in the field pattern. Limited to magnetic materials.
- *Radiography.* In the case of x–ray or γ–ray radiography, a portable source is used to irradiate the component, and the absorption assessed from the image on a sensitive film on the opposite side of the component from the source. Cracks, which absorb less radiation, appear as dark areas on the film. The method is sensitive, and may be used to detect internal cracks. However, poor crack orientation may produce inferior images.
- *Ultrasonics.* A probe emits a high frequency sound wave into the component, which is reflected by surfaces, including internal cracks. The time taken for transmission and reflection of a pulse is normally indicated on an oscilloscope. This may be interpreted as a distance through the component, and hence allow the crack to be properly located.

The selection of appropriate NDI methods is very important. Accessibility of the part and operator experience are key factors for successful NDI. Ultrasonics can be used before machining wrought stock to detect internal flaws. Radiography is less sensitive than ultrasonics, but it may be easier to apply and can disclose internal defects that often accompany cracks (inclusions, porosity, and voids). Penetrant inspection is common for surface flaw detection. Smeared material on machined surfaces that hides a crack–like flaw should be removed with etchant. If a fine finish is required, penetrant inspection before final machining would allow etching. More complicated than penetrant inspection, eddy current inspection should be used if etching is detrimental or if the surface is coated. Magnetic particle inspection has limited reliability to detect small flaws. [49]

Table 7. Selected assumed initial flaw sizes from MSFC–STD–1249.

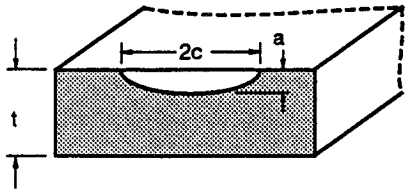

Method	thickness	a (in)	2c (in)
Penetrant	t < 0.075 in	0.025	0.25
		0.04	0.2
		0.075	0.175
	t ≥ 0.075 in	0.025	0.25
		0.04	0.2
		0.075	0.15
Eddy Current	t ≥ 0.020 in	0.01	0.1
		0.02	0.1
		0.05	0.1
Magnetic Particle	t ≥ 0.070 in	0.0375	0.375
		0.055	0.275
		0.125	0.25

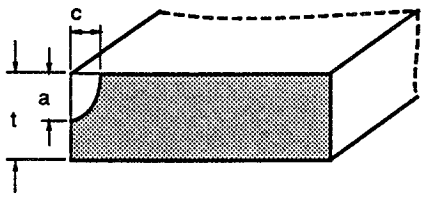

Method	thickness	a (in)	c (in)
Penetrant	t < 0.075 in	t	0.125
	t ≥ 0.075 in	0.075	0.1
Eddy Current	t ≥ 0.020 in	0.02	0.05
Magnetic Particle	t ≥ 0.070 in	0.07	0.15

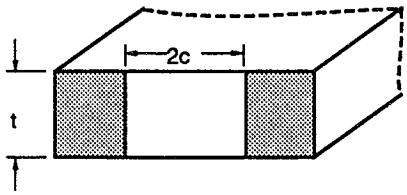

Method	thickness	a (in)	2c (in)
Penetrant	t < 0.075 in	t	0.2
	t ≥ 0.075 in	t	0.15
Eddy Current	t ≥ 0.020 in	t	0.1
Magnetic Particle	t ≥ 0.070 in	t	0.25

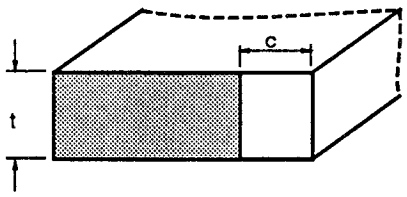

Method	thickness	a (in)	c (in)
Penetrant	t < 0.075 in	t	0.1
	t ≥ 0.075 in	t	0.1
Eddy Current	t ≥ 0.020 in	t	0.05
Magnetic Particle	t ≥ 0.070 in	t	0.25

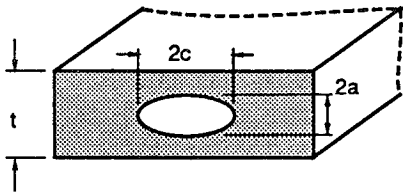

Method	thickness	2a (in) ---- 2c (in)
Ultrasonic	t ≥ 0.3 in	equivalent area of 0.2 in diameter circle
Radio-graphy	t < 0.05 in	0.7 t ---- max {0.15,t}
	t ≥ 0.05 in	max {0.7 t,0.025} ---- 0.15

6.2.2 Proof Testing

Proof testing has been extensively used to screen out gross material and manufacturing defects. These defects are eliminated under controlled circumstances to prevent catastrophic failure during actual service. Proof testing is a useful supplement to conventional NDI when the maximum permissible flaw can escape detection by NDI, when a structure is too large to make complete NDI feasible, and when the geometry is too complex to make NDI reliable.

Proof testing is typically performed with a pressure that exceeds the maximum operating pressure subject to the requirement that the nominal stresses remain below 85 percent of the ultimate strength of the material. Proof testing should be performed in the actual operating environment. However, it is not always possible to do this because of safety and cost constraints. An environmental correction factor that accounts for the differences between the material's response in the proof environment and the material's response in the actual operating environment should be applied. In cases where the required proof test factor in the actual environment is very large, it may be desirable to proof test at lower temperatures where the material's fracture toughness is reduced. The resulting proof test factor will also be reduced.

For a proof test to be effective, the structure must be made of a material that acts in a brittle manner when the service load and environment is applied. For a brittle material undergoing proof testing, the existing cracks below the critical flaw size do not grow to failure. In this regard, the proof test can be seen as a destructive inspection because only existing cracks equal to or larger than the critical flaw size will grow to failure. It is assumed that no crack survives that is larger than the critical flaw size determined for the proof cycle. Therefore, a margin of life is obtained because the service load is smaller than the proof load. This margin of life is the number of cycles it takes to grow the largest flaw size that could survive proof to the critical flaw size at the service conditions. The reader should consult Reference [52] for more details.

7 MISCELLANEOUS TOPICS

7.1 Relationship Between K_I and k_t

The dimensionless stress concentration factor, k_t, accounts for the increase in nominal stress due to geometry: $\sigma_{max} = k_t \sigma$. Both notch length and notch root radius influence k_t. The stress intensity factor, K_I, accounts for both geometric variables (crack length explicitly and crack–tip radius implicitly because the radius is assumed to be very sharp) and the stress level. K_I provides the complete stress and displacement field near the crack tip, whereas, k_t provides the useless result $k_t = \infty$ at the crack tip regardless of notch size and shape and stress level.

It is often advantageous to relate the stress concentration factor solution of a notch to the stress intensity factor solution of a crack because of the large number of existing stress concentration solutions for notches. [16] Recall that the stress σ_{yy} directly ahead of the crack is:

$$\sigma_{yy} = \frac{K_I}{\sqrt{2\pi r}}. \tag{54}$$

If this equation is used to approximate the stress near a notch of root radius ρ and root stress σ_{max}, then

$$K_I = C\sigma_{max}\sqrt{\rho}, \tag{55}$$

as $\rho \rightarrow 0$. For the notch solution of an elliptical hole under uniform tension:

$$\sigma_{max} = \left(1 + 2\sqrt{\frac{a}{\rho}}\right)\sigma, \tag{56}$$

where σ is the remote stress, a is the semimajor axis, and ρ is the semiminor axis. As the semiminor axis becomes small, it becomes the root radius of the crack tip, while the semimajor axis becomes the crack length. In equation 56, the stress concentration factor k_t is:

$$k_t = 1 + 2\sqrt{\frac{a}{\rho}}. \tag{57}$$

Substituting equation 56 into equation 55 and taking the limit as $\rho \rightarrow 0$ yields:

$$K_I = \lim_{\rho \to 0} \left[C\sigma \left(1 + 2\sqrt{\frac{a}{\rho}} \right) \sqrt{\rho} \right] = 2C\sigma\sqrt{a}. \tag{58}$$

Comparing the above equation to $K_I = \sigma\sqrt{\pi a}$, the constant $C = \sqrt{\pi}/2$. Therefore, K_I can be computed from a corresponding notch solution:

$$K_I = \lim_{\rho \to 0} \left[\frac{\sqrt{\pi}}{2} \sigma_{max} \sqrt{\rho} \right]. \tag{59}$$

This equation can be very useful in estimating K_I for many notch problems. [5, 9]

7.2 Leak Before Burst

The condition of leak before burst (LBB) occurs when initial flaws in a pressure vessel safely grow through the pressure wall without causing immediate catastrophic failure. The transition of surface cracks into through cracks is the basic concern of LBB. The LBB condition cannot be met for arbitrarily large flaw sizes because for a given pressure, there is always a flaw size large enough to cause the pressure vessel to burst. A reasonable approach to leak before burst of a thin-wall pressure vessel is to consider the size of the assumed initial flaw from the NDI method selected for the pressure vessel. M.F. Kanninen [46] developed the following approach.

Suppose the crack length is long compared to the crack depth as shown in Figure 23. This assumption will be conservative for all crack aspect ratios. The initiation of unstable crack growth in the radial direction (through the thickness) occurs when:

$$K_{Ic} = 1.12 \frac{pR}{t} \sqrt{\pi a} \sqrt{\sec\left(\frac{\pi a}{2t}\right)}. \tag{60}$$

At crack breakthrough, the through crack will likely have a length equal to the length of the original surface flaw. The critical condition for unstable crack growth is:

$$K_c = \frac{pR}{t} \sqrt{\pi c} \sqrt{1 + 1.61 \frac{c^2}{Rt}}. \tag{61}$$

In equation 60, K_{Ic}, the plane strain fracture toughness, is used for the failure condition because the surface crack can be highly constrained. In equation 61, K_c, the plane stress fracture toughness, is used for the failure condition because the through crack for a thin wall undergoes plane stress constraint.

If the two equations are combined, then the boundary between leak and burst behavior of a pressure vessel can be determined using:

$$\left[1 + 1.61\frac{t}{R}\left(\frac{c}{t}\right)^2\right]\frac{c}{t} = 1.25\left(\frac{K_c}{K_{Ic}}\right)^2\frac{a}{t}\sec\left(\frac{\pi a}{2t}\right). \tag{62}$$

The ratio K_c/K_{Ic} can have a large effect on the boundary of the leak regime as shown in Figure 24.

If NDI is not performed on the pressure vessel, then the stress intensity factor for an axial through crack in a cylinder:

$$K_I = \frac{pR}{t}\sqrt{\pi c}\sqrt{1 + 1.61\frac{c^2}{Rt}} \tag{63}$$

must be compared with K_c. The assumptions $2c = 10t$ and $R/t = 10$ for a thin–wall vessel lead to: $K_I = 255\, p\, \sqrt{t}$. If $K_I < K_c$, then the LBB condition is met. When leakage cannot be tolerated, design for LBB is not sensible. Safe–life design should be used with the end of service life defined as leakage instead of unstable crack growth.

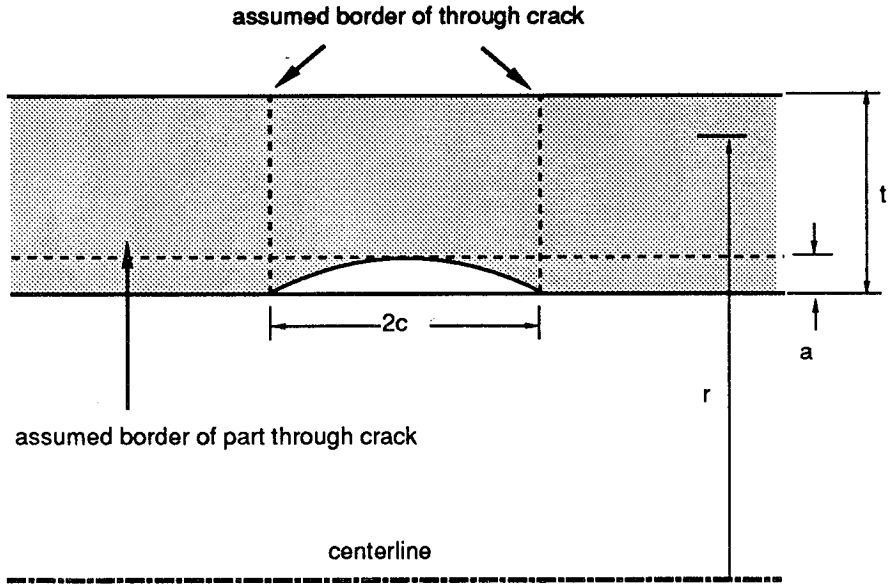

Figure 23. Conservative LBB geometry.

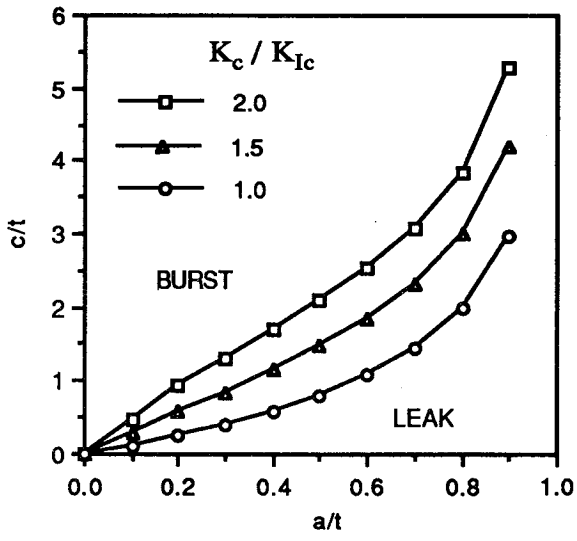

Figure 24. Leak and burst regimes for $R/t = 10$.

8 EXAMPLE PROBLEMS AND PRACTICE SET

8.1 Example Problems

8.1.1 Stress Intensity Factor Calculation

A 6061–T6 aluminum alloy plate is 10.0–in wide and 0.25–in thick. The plate's fracture toughness K_c is 27 ksi$\sqrt{\text{in}}$ and the operating load P is 90,000 lb. Is the plate safe in the presence of a 0.5–in edge crack? If not, what is the critical load?

Assume that the stress due to P is uniformly distributed across the plate:

$$\sigma = \frac{P}{A} = \frac{90,000\text{ lb}}{(0.25\text{ in})(10.0\text{ in})} = 36.0\text{ ksi}.$$

The stress intensity factor is given by equation 14:

$$K_I = \lambda\sigma\sqrt{\pi a}.$$

For $\frac{a}{W} = 0.05$ and $\lambda = 1.1343$ (section 3.4, case 2), K_I becomes:

$$K_I = 1.1343(36\text{ ksi})\sqrt{\pi(0.5\text{ in})} = 51\text{ ksi}\sqrt{\text{in}}.$$

Therefore, the plate is unsafe with a 0.5–in crack because $K_I > K_c$.

To calculate the critical load for the 0.5–in crack, let $K_I = K_c$ and $a = a_c$, then calculate the correction factor λ and solve equation 14 for the critical stress:

$$\sigma_c = \frac{K_c}{\lambda\sqrt{\pi a_c}}.$$

Substituting the previously determined quantities into the above equation:

$$\sigma_c = \frac{27\text{ ksi}\sqrt{\text{in}}}{1.1343\sqrt{\pi(0.5\text{ in})}} = 19\text{ ksi}.$$

The critical load is:

$$P_c = \sigma_c A = (19.0\text{ ksi})(0.25\text{ in})(10\text{ in}) = 47,500\text{ lb.}$$

Therefore, the plate fails at a much lower load than the operating load. To calculate the critical flaw size at the operating load, use equation 14 with $\sigma = \sigma_c$ and $K_I = K_c$:

$$a_c = \frac{1}{\pi}\left(\frac{K_c}{\lambda\sigma_c}\right)^2,$$

where λ is a function of a_c. The critical crack length was iteratively determined to be 0.14 in, well below the planned 0.5 in. The following options could be considered in the design change:

- Use a material with a higher K_c value.
- Lower the operating stress.
- Change the component configuration.
- Improve the inspection by increasing the accessibility of the part, allowing the use of a more sensitive technique, or decreasing the period between inspection.

8.1.2 Factor of Safety for Critical Stress

A high strength steel alloy plate 10–in wide and 1.875–in thick may contain surface cracks. The planned NDI technique can detect a surface crack 0.375–in deep and 0.75–in long. The material's fracture toughness is $95\text{ ksi}\sqrt{\text{in}}$. If the allowable stress for the material is 60 ksi, determine the factor of safety for the plate.

Table 1 can be used to determine the correction factor λ_t for a semi–elliptical surface crack. For $\frac{a}{c} = 1$ and $\frac{a}{t} = 0.2$, $\lambda_t = 1.174$ at $\phi = 0$ and $\lambda_t = 1.049$ at $\phi = \pi/2$.

Solving the stress intensity factor equation for the critical stress gives:

$$\sigma_c = \frac{K_c}{\lambda_{tot}\sqrt{\pi a_c}} \tag{64}$$

where $\lambda_{tot} = (\lambda_t \lambda_w)/\Phi$. The finite width correction (calculated from equation 36) is $\lambda_w = 1.0007$. For $a/c = 1$, the elliptical integral is $\Phi = \pi/2$. Combining these values

gives $\lambda_{tot} = 0.7479$ at $\phi = 0$ and $\lambda_{tot} = 0.6683$ at $\phi = \pi/2$. Using the largest total correction factor will give the lowest value for critical stress:

$$\sigma_c = \frac{95\ \text{ksi}\sqrt{\text{in}}}{0.7479\sqrt{\pi(0.375\ \text{in})}} = 117\ \text{ksi}. \tag{65}$$

The factor of safety is:

$$F.S. = \frac{\sigma_c}{\sigma} = \frac{117\ \text{ksi}}{60\ \text{ksi}} = 1.95. \tag{66}$$

8.1.3 Crack Growth in a Plate

A large, wide plate (use $\lambda = 1$) contains a 0.20–in through crack. The plate is subjected to a cyclic operating stress that varies between 5 and 25 ksi. The fatigue crack growth rate can be expressed using Equation 45 with $C = 5 \times 10^{-10}$ and $n = 4.0$ (ΔK is expressed in $\text{ksi}\sqrt{\text{in}}$, and da/dN in inches/cycle). K_c is $60.0\text{ksi}\sqrt{\text{in}}$ and ΔK_{th} is $10.0\text{ksi}\sqrt{\text{in}}$. (a) Determine the number of cycles required for the crack to grow from an initial size, $2a_i$, of 0.20 in to a length of 0.5 in. To determine the number of cycles, equation 45 must be integrated:

$$\frac{da}{dN} = C(\Delta K)^n = C(\Delta\sigma\sqrt{\pi a})^n.$$

Solving for the number of cycles:

$$N_f = \int_0^{N_f} dN = \frac{1}{C(\Delta\sigma\sqrt{\pi})^n} \int_{a_i}^{a_f} \frac{da}{(\sqrt{a})^n}.$$

Substituting values,

$$N_f = \frac{1}{5 \times 10^{-10}(20\sqrt{\pi})^{4.0}} \int_{0.1}^{0.25} \frac{da}{(\sqrt{a})^{4.0}}.$$

Solving the integration yields:

$$\begin{aligned} N_f &= -\frac{1}{5 \times 10^{-10}(20\sqrt{\pi})^{4.0}} \left[(0.25)^{-1.0} - (0.1)^{-1.0}\right], \\ N_f &= 7,600\ \text{cycles}. \end{aligned}$$

(b) Determine the number of cycles for the crack to grow from an initial length of 0.20 in to failure. Failure will occur when the crack reaches the critical length for the maximum stress of 25 ksi. To determine the critical crack length at this stress, let $K_I = K_c$:

$$K_c = \sigma_{max}\sqrt{\pi a_c}.$$

Solving for a_c yields:

$$a_c = \frac{K_c^2}{\pi \sigma_{max}^2} = \frac{(60)^2}{\pi(25)^2} = 1.83\,\text{in}.$$

To determine the number of cycles it takes for the crack to grow from its initial half–length, $a_i = 0.1$ in, to its critical half–length, $a_c = 1.83$ in, let $a_f = a_c$ and $N_f = N_c$ in the equation for N_f in part (b),

$$N_c = \int_0^{N_c} dN = \frac{1}{C(\Delta\sigma\sqrt{\pi})^n}\int_{a_i}^{a_c}\frac{da}{(\sqrt{a})^n}.$$

Substituting values and integrating yields:

$$\begin{aligned} N_f &= -\frac{1}{5\times 10^{-10}(20\sqrt{\pi})^{4.0}}\left[(1.83)^{-1.0} - (0.1)^{-1.0}\right], \\ N_f &= 11,970 \text{ cycles}. \end{aligned}$$

A total of 11,970 cycles are required for the crack to grow from a half–length of 0.1 in to failure. Growing the crack to 0.25 in required 7,600 cycles, and only 4,371 additional cycles were required to grow the crack from $a = 0.25$ in to its critical value of $a_c = 1.83$ in. As the crack grows longer, the stress intensity factor increases causing the crack growth rate to increase. Figure 25 is a plot of the number of cycles required to grow the crack to various lengths.

In this example, the correction factor λ, in the expression for the stress intensity factor was unity. In general, the correction factor depends on the crack length and geometry making the integration indicated in equation 51 more complicated than this example. In many problems, it is possible to treat λ as a constant for a small interval

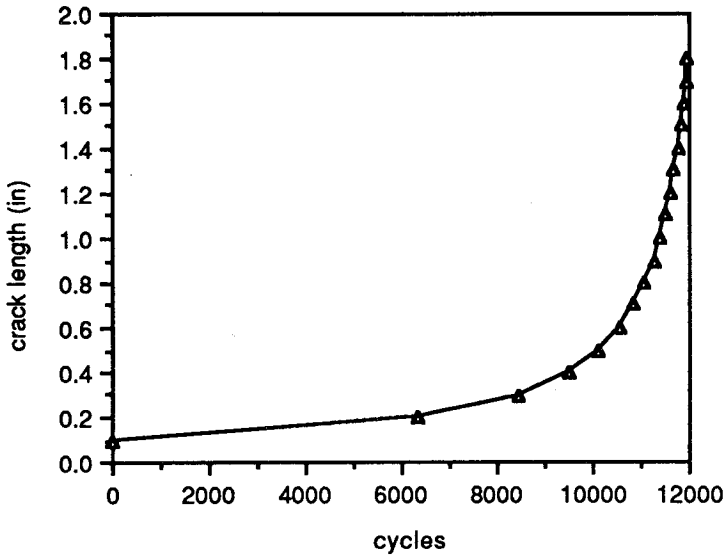

Figure 25. Fatigue crack growth of a center cracked plate.

of crack extension ($\Delta a \approx 0.05$ in for example). Then a revised value of λ can be used for the next interval of crack growth. This process can be continued, assuming λ is a constant for each interval of growth, until the required crack length is reached.

(c) If the plate is to be designed for no crack growth, what is the crack size that must be screened using NDI? In this case,

$$\Delta K = \lambda \Delta\sigma \sqrt{\pi a}, \tag{67}$$

must be solved for $a = a_{th}$ by letting $\Delta K = \Delta K_{th}$:

$$a_{th} = \frac{1}{\pi}\left(\frac{\Delta K_{th}}{\lambda \Delta\sigma}\right)^2. \tag{68}$$

For a wide plate, the correction factor λ is unity and the threshold crack size is:

$$a_{th} = \frac{1}{\pi}\left(\frac{10}{20}\right)^2 = 0.08 \text{ in} \tag{69}$$

Therefore, NDI must reliably detect cracks as small as 0.08 in to ensure no crack growth in the plate.

8.1.4 Flaw–screening Proof Test Factor

A 10–in wide, 1–in thick plate made of 2219–T87 aluminum alloy is cyclically loaded with a tensile stress ranging between 0 to 15 ksi. The plate is part of a structure that must withstand 10,000 cycles of operation. Assuming that the most likely existing crack is a through crack in the center of the plate, determine the proof test factor necessary to ensure that the plate will withstand 40,000 cycles (10,000 cycles $\times$ scatter factor of 4).

For 2219-T87 at room temperature, the yield strength is $\sigma_{ys} = 66$ ksi and the fracture toughness is $K_{Ic} = 35 \text{ ksi}\sqrt{\text{in}}$. The Paris equation constants are $C = 0.109 \times 10^{-9} \text{in.}/(\text{ ksi}\sqrt{\text{in}})^n$ and $n = 3.709$. Because the fracture toughness and number of cycles to failure are known, it is possible to iteratively determine the maximum initial crack size by guessing an initial flaw size and then comparing the cycles to failure with 40,000 cycles. A guess of $a_i = 0.5$ in yielded 57,809 cycles to failure, implying that the desired initial flaw size is larger. Guessing a larger size, $a_i = 0.75$ in, gives 29,267 cycles to failure. Therefore, the desired initial flaw size is bounded between 0.5 and 0.75 in. A final guess, $a_i = 0.6$ in, yielded 43,672 cycles to failure. This 0.6–in

crack size is the approximate initial flaw size for fatigue life that must be screened by the proof test.

In Figure 26, the proof factor determination is shown. For a proof stress of 20 ksi, the proof factor of 1.33 is calculated. This proof stress, the critical flaw size is $a_c = 0.9332$ in. Using this crack size as the initial flaw size for the operating stress yields a life of 17,944 cycles. Because this critical flaw size is larger than the maximum initial flaw size needed for 40,000 cycles, a larger proof factor must be used. For a proof stress of 25 ksi, the resulting proof factor is 1.67, and the critical flaw size is $a_c = 0.6124$ in. Using this crack size as the initial flaw size for the operating stress of 15 ksi yields 42,266 cycles to failure.

8.1.5 Solid Rocket Motor Case Failure

A NASA–owned solid rocket motor case failed during proof testing on April 11, 1965. The 260–in diameter motor case failed at a hydrotest pressure of 542 psi, well before reaching the planned proof pressure of 960 psi. The motor case was constructed of grade 250 (nominal yield strength of 250 ksi) maraging steel and joined by submerged arc automatic welding. Of the 975 ft of welds in the case, 330 ft of repair welds were required. The failure investigation revealed that the failure originated from a crack–like defect undetected by NDI techniques before aging and hydrotest. Embedded in the wall of the motor case and oriented longitudinally, the defect causing failure was approximately 1.4–in long and 0.10– to 0.22–in wide. The thickness at the fracture origin was 0.73 in. The defect was in the heat–affected zone of a longitudinal submerged arc weld on the cylindrical section of the motor case in an area that had been repaired by a manual gas–tungsten–arc (TIG) weld. Additionally, four other significant undetected defects were found under manual TIG weld repairs. One defect, in the same longitudinal weld as the defect causing the failure, was large enough to act as a secondary failure origin. The other defects were found during reinspection of the welds after the hydrotest failure.

The actual yield strength for base plate was 240 ksi, and the applied stress at failure was 96.5 ksi. Using a crack size of 1.4–in long and 0.1– to 0.22–in wide and a simple stress intensity factor solution,

$$K_I = \sigma \frac{\sqrt{\pi a}}{\Phi} \sqrt{sec\left(\frac{\pi a}{t}\right)}, \tag{70}$$

with Φ taken from Table 2. The calculated critical stress intensity factors were 38.1 and 48.8 ksi$\sqrt{\text{in}}$. The fracture toughness, K_{Ic}, based on specimens prepared from

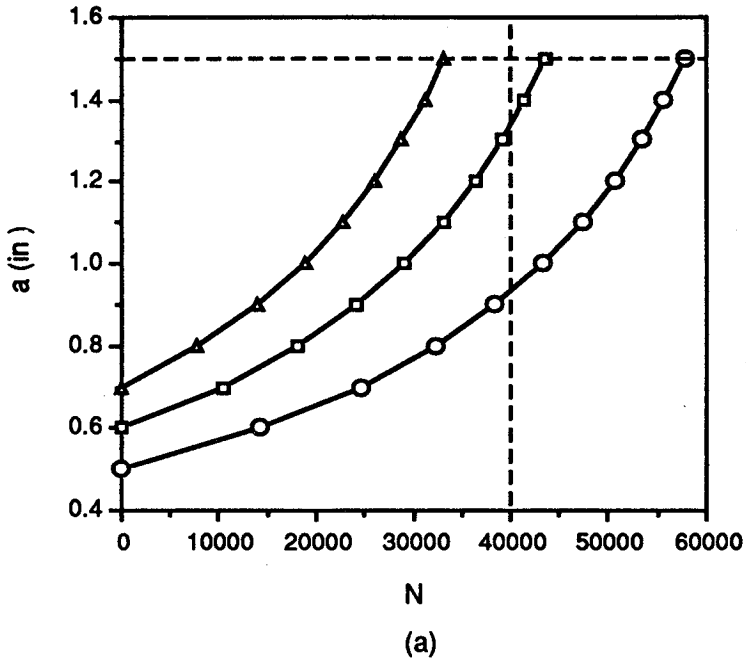

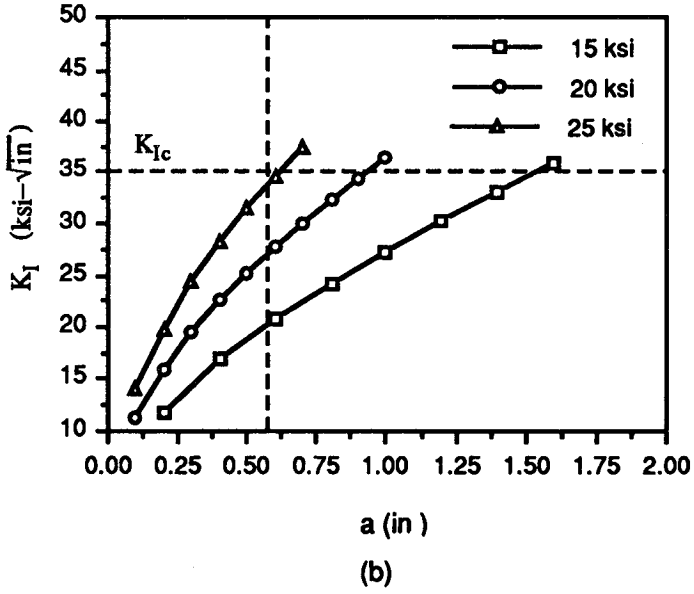

Figure 26. Determination of proof factor for a center cracked plate.

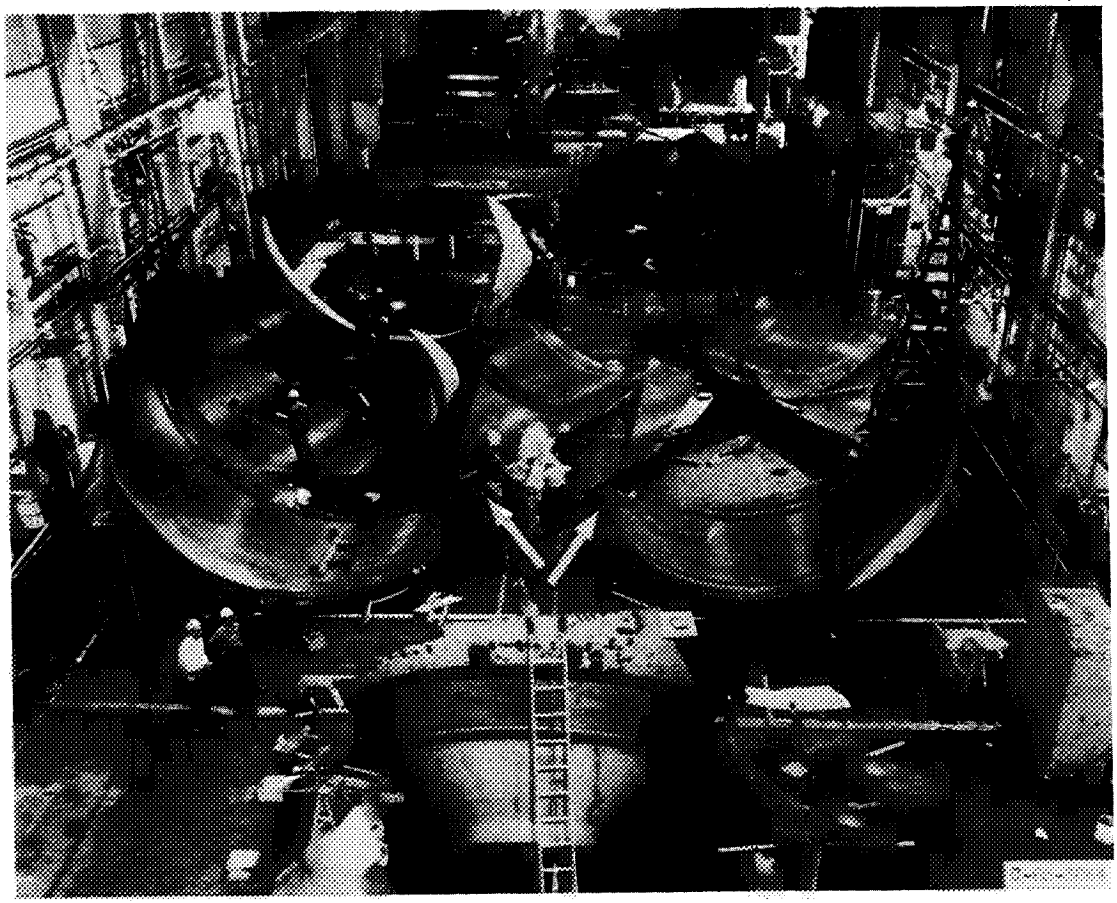

Figure 27. Reassembled fragments from ruptured solid rocket motor case (arrows indicate origin of failure).

the heat affected zone (HAZ) of a submerged arc weld was measured to be 77 ksi$\sqrt{\text{in.}}$ This value did not account for a TIG–manual repair weld. To account for the repair weld, K_{Ic} for a section containing a known defect was estimated to be 49.3 ksi$\sqrt{\text{in}}$ — showing excellent agreement with the calculated critical stress intensity factors.

The failure investigation included a limited test program to determine the sensitivity of radiographic and ultrasonic procedures for detecting tight fatigue cracks in flat plate specimens. The investigation committee found that these NDI methods were much less sensitive and reliable than originally expected. The committee concluded that more research was required on NDI techniques for detection of small defects in thick sections before the materials and weld procedures could be successfully used for solid rocket motor cases.

The fracture toughness of the submerged arc welds was inadequate to tolerate the large crack–like weld defects. It was unrealistically believed that smaller defects could be detected with high reliability by the NDI procedures used. The fracture toughness would have been sufficient if no defects had been present larger than the expected detectable size. Regardless of improvements in the reliability of the NDI techniques,

using a lower strength steel with a higher toughness would have been better. The defect that failed the grade 250 motor case would not have failed a grade 200 (nominal yield strength of 200 ksi) maraging steel motor case because fracture toughness for grade 200 is 150 ksi$\sqrt{\text{in}}$. Using a failure stress of 100 ksi, the lower strength case could tolerate a 1.4–in through crack. In fact, two grade 200 motor cases were successfully proof tested and test fired, developing thrusts in excess of six million pounds. [53, 54]

8.2 Practice Set

1. A large aluminum plate has a fracture toughness of 25.3 ksi$\sqrt{\text{in}}$. If a 0.5–in edge crack develops in the plate, what is the critical stress for the plate? *(Ans. 18 ksi.)*

2. If the plate in problem 1 has an operating stress of 30 ksi, what is the critical crack length? *(Ans. 0.18 in.)*

3. An edge crack is expected to grow from a 14–mm diameter fastener hole in a large plate with a fracture toughness of 101 MPa$\sqrt{\text{m}}$. The smallest crack which can be detected is 2 mm. If the plate has a design stress of 420 MPa, what is the safety factor based on fracture toughness? *(Ans. 1.4.)*

4. A 0.5–in thick connecting arm is assumed to develop an edge crack as shown below. The smallest crack which can be reliably detected by the planned NDI method is 0.25 in. The material has a fracture toughness of 60 ksi$\sqrt{\text{in}}$. What is the critical load P assuming the existence of the smallest detectable crack? *(Ans. 4,400 lb.)*

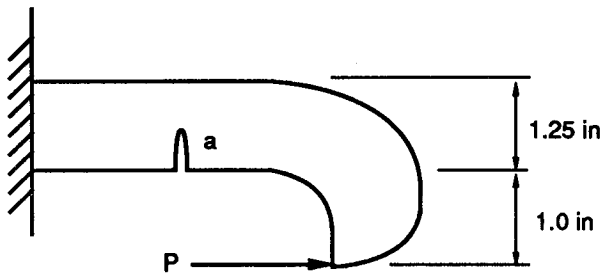

5. A cylindrical pressure tank is assumed to develop a 20–mm axial crack through the thickness. The tank has a liner to prevent leakage at the crack. The diameter of the tank is 800 mm and the wall thickness is 5 mm. If the fracture toughness of the tank material is 40 MPa$\sqrt{\text{m}}$, what is the maximum internal pressure the tank can withstand? *(Ans. 2.9 MPa.)*

6. A total error of 10 percent exists in the stress analysis and stress intensity factor analysis of a component. If the fatigue crack growth rate $\frac{da}{dN}$ is roughly proportional to $(\Delta K)^4$, estimate the error in the calculated crack growth rate of the component. *(Ans. 45 percent.)*

7. During a proof test, a large cylindrical pressure vessel prematurely failed at an internal pressure of 5.29 MPa. Inspection of the fracture surfaces revealed an embedded crack in an axially–oriented weld seam 41 mm long and 4.1 mm deep. The inside diameter of the pressure vessel was 635 cm and the wall thickness was 24 mm. If the fracture toughness of the material was 55.5 MPa$\sqrt{\text{m}}$, was the undetected crack large enough to cause failure? *(Ans. Yes, the critical stress was 460 MPa and the proof stress was over 700 MPa.)*

8. A cylindrical pressure vessel has a wall thickness of 22 mm and an inside diameter of 558 cm. The smallest crack that can be reliably detected using NDI has a length of 8 mm and a depth of 4 mm. The material's toughness is 66 MPa$\sqrt{\text{m}}$ and the internal operating pressure is 4.8 MPa. If the crack is oriented axially, what is the factor of safety against brittle fracture? *(Ans. 1.4.)*

9. A large plate is being designed for the presence of an edge crack. The plate is subjected to an alternating load that varies sinusoidally from a minimum stess of 10 ksi to a maximum stress of σ_{max}. If the initial crack is 0.125–in long and the stress intensity threshold is 8 ksi$\sqrt{\text{in}}$, what is the allowable value of σ_{max} for a nonpropagating crack? *(Ans. 21 ksi.)*

10. The plate in problem 9 has a toughness of 32 ksi$\sqrt{\text{in}}$. The Paris equation coefficients are $C = 1.5 \times 10^{-11}$ and $n = 3.1$. If the plate is to be designed for sinusoidally varying load having a minimum stress of 10 ksi and a maximum stress of 25 ksi, how many load cycles will the plate withstand before the crack grows from its initial length of 0.125 in to failure? *(Ans. 5,000,000 cycles.)*

REFERENCES

[1] Forman, R.G., Shivakumar, V., Newman, J.C., Jr., Piotrowski, S.M., and Williams, L.C.: "Development of the NASA/FLAGRO Computer Program." Fracture Mechanics: 18th Symposium, ASTM STP 945, pp. 781–803 Philadelphia: 1988.

[2] Harris, D.O., Eason, E.D., Thomas, J.M., Bianca, C.J., and Salter, L.D.: "NASCRAC — A Computer Code for Fracture Mechanics Analysis of Crack Growth." AIAA-87-0847-CP, AIAA/ASME/ASCE/AHS 28th Structures, Structural Dynamics and Materials Conference, pp. 662–667, Monterey, CA, April 6–8, 1987.

[3] Broek, D.: "Elementary Engineering Fracture Mechanics." Martinus Nijhoff, Dordrecht, The Netherlands, 1987.

[4] Ewalds, H.L., and Wanhill, R.J.H.: "Fracture Mechanics." Edward Arnold, Baltimore, 1986.

[5] Anderson, T.L.: "Fracture Mechanics: Fundamentals and Applications." CRC Press, Boston, 1991.

[6] Collins, J.A.: "Failure of Materials in Mechanical Design: Analysis, Prediction, Prevention." Wiley–Interscience, New York, 1981.

[7] Bannantine, J.A., Comer, J.J., and Handrock, J.L.: "Fundamentals of Metal Fatigue Analysis." Prentice Hall, Englewood Cliffs, NJ, 1990.

[8] Wulpi, D.J.: "Understanding How Components Fail." American Society for Metals, Metals Park, OH, 1985.

[9] Inglis, C.E.: "Stresses in Plate Due to the Presence of Cracks and Sharp Corners." Transactions of the Institution of Naval Architects, Series A, vol. 55, pp. 219–230, London, 1913.

[10] Griffith, A.A.: "The Phenomena of Rupture and Flow in Solids." Philosophical Transactions of the Royal Society, Series A, vol. 221, pp. 163–198, London, 1920.

[11] Irwin, G.R.: "Fracture Dynamics." Fracturing of Metals, Cleveland, American Society for Metals, 1948.

[12] Orowan, E.: "Fracture and Strength of Solids." Report of Progess in Physics, vol. 12, 1949.

[13] Irwin, G.R.: "Analysis of Stresses and Strains Near the End of a Crack Tranversing a Plate." Journal of Applied Mechanics, vol. 24, pp. 361–364, September 1957.

[14] Williams, M.L.: "On the Stress Distribution at the Base of a Stationary Crack." Journal of Applied Mechanics, vol. 24, pp. 109–114, March 1957.

[15] Paris, P.C., Gomez, R.E., and Anderson, W.E: "A Rational Analytic Theory of Fatigue." The Trend in Engineering, vol. 13, No. 1, pp. 9–14, January 1961.

[16] Peterson, R.E.: "Stress Concentration Factors." Wiley–Interscience, New York, 1974.

[17] Cartwright, D.J., and Rooke, D.P.: "Approximate Stress Intensity Factors Compounded from Known Solutions." Engineering Fracture Mechanics, vol. 6, pp. 563–571, 1974.

[18] Cartwright, D.J., and Rooke, D.P.: "Green's Functions in Fracture Mechanics." Fracture Mechanics: Current Status, Future Prospects, Cambridge University Conference Proceedings, pp. 91–123, March 16, 1979.

[19] Liebowitz, H., and Moyer, E.T., Jr.: "Finite Element Methods in Fracture Mechanics." Computers and Structures, vol. 31, No. 1, pp. 1–9, 1989.

[20] Gerstle, W.H., and Abdalla, J.E., Jr.: "Finite Element Meshing Criteria for Crack Problems." Fracture Mechanics: 21st Symposium, ASTM STP 1074, pp. 509–521, ASTM, Philadelphia, 1990.

[21] Mikkola, T.P.J., and Niemi, H.: "Quality Assurance for Fracture Mechanical Finite Element Analyses." Computers and Structures, vol. 40, No. 2, pp. 271–279, 1991.

[22] Cruse, T.A.: "Boundary Element Analysis in Computational Fracture Mechanics." Kluwer Academic, Dordrect, The Netherlands, 1988.

[23] Thomas, J.M., Harris, D.O., and Besuner, P.M.: "Fracture Mechanics Life Technology," AIAA-86-0982-CP, AIAA/ASME/ASCE/AHS 27th Structures, Structural Dynamics and Materials Conference, pp. 562–578, San Antonio, May 19–21, 1986.

[24] Mullinix, B.R., and Smith, D.G.: "Fracture Mechanics Design Handbook." Technical Report TL-77-8, U.S. Army Missile Research and Development Command, August 1977.

[25] Tada, H., Paris, P., and Irwin, G.: "The Stress Analysis of Cracks Handbook." Paris Productions, St. Louis, 1985.

[26] Sih, G.C.: "Handbook of Stress Intensity Factors." Lehigh University, Bethlehem, PA, 1973.

[27] Rooke, D.P., and Cartwright, D.J.: "Compendium of Stress Intensity Factors." Her Majesty's Stationary Office, London, 1976.

[28] Raju, I.S., and Newman, J.C., Jr.: "Stress–Intensity Factors for a Wide Range of Semi–Elliptical Surface Cracks in Finite–Thickness Plates." Engineering Fracture Mechanics, vol. 11, pp. 817–829, 1979.

[29] Newman, J.C., Jr., and Raju, I.S.: "An Empirical Stress-Intensity Factor Equation for the Surface Crack." Engineering Fracture Mechanics, vol. 15, No. 1–2, pp. 185–192, 1981.

[30] Newman, J.C., Jr., and Raju, I.S.: "Stress-Intensity Factor Equations for Cracks in Three–Dimensional Finite Bodies Subjected to Tension and Bending Loads." NASA TM–85793, April 1984.

[31] "Damage Tolerant Design Handbook." Metals and Ceramics Information Center, Battelle, Columbus Laboratories, Columbus, OH, January 1975.

[32] "Aerospace Structural Metals Handbook," Metals and Ceramics Information Center, Battelle, Columbus Laboratories, Columbus, OH, 1988.

[33] "Metallic Materials and Elements for Aerospace Vehicle Structures," MIL–HDBK-5F, 1990.

[34] Hudson, C.M., and Seward, S.K.: "A Compendium of Sources of Fracture Toughness and Fatigue Crack Growth Data for Metallic Alloys." International Journal of Fracture, vol. 14, pp. R151–R184, 1978.

[35] Hudson, C.M., and Seward, S.K.: "A Compendium of Sources of Fracture Toughness and Fatigue Crack Growth Data for Metallic Alloys - Part II." International Journal of Fracture, vol. 20, pp. R59–R117, 1982.

[36] Hudson, C.M., and Seward, S.K.: "A Compendium of Sources of Fracture Toughness and Fatigue Crack Growth Data for Metallic Alloys - Part III." International Journal of Fracture, vol. 39, pp. R43–R63, 1989.

[37] Hudson, C.M., and Ferrainolo, J.J.: "A Compendium of Sources of Fracture Toughness and Fatigue Crack Growth Data for Metallic Alloys - Part IV." International Journal of Fracture, vol. 48, pp. R19–R43, 1991.

[38] Chambers, A.E., and Sinclair, G.B.:"On Obtaining Fracture Toughness Values From the Literature." International Journal of Fracture, vol. 30, pp. R11–R15, 1986.

[39] American Society for Testing and Materials, "E 399-90 Standard Test Method for Plane–Strain Fracture Toughness of Metallic Materials." 1991 Annual Book of ASTM Standards, vol. 03.01, 1991.

[40] American Society for Testing and Materials, "E 647-91 Standard Test Method for Measurement of Fatigue Crack Growth Rates." 1991 Annual Book of ASTM Standards, vol. 03.01, 1991.

[41] Sinclair, G.B., and Pieri, R.V.: "On Obtaining Fatigue Crack Growth Parameters From the Literature." Internationl Journal of Fatigue, vol. 12, No. 1, pp. 57–62, 1990.

[42] Schwartz, B.J., Engsberg, N.G., and Wilson, D.A.: "Development of a Fatigue Crack Propagation Model of Incoloy 901." Fracture Mechanics: 15th Symposium, ASTM STP 833, ASTM, pp. 218–241, Philadelphia, 1984.

[43] Broek, D.: "A Similitude Criterion for Fatigue Crack Growth Modeling." Fracture Mechanics: 16th Symposium, ASTM STP 868, ASTM, pp. 347–360, Philadelphia, 1985.

[44] Seetharm, S.A., and Dash, P.K.: "Delta–K Correlation of Fatigue Crack Growth Rates Under General Monotonic Loading." International Journal of Fracture, vol. 52, pp. R3–R8, 1991.

[45] Saxena, A.: "Limits of Linear Elastic Fracture Mechanics in the Characterization of High–Temperature Fatigue Crack Growth." Basic Questions in Fatigue: Yolume II, ASTM STP 924, pp. 27–40, ASTM, Philadelphia, 1988.

[46] Kanninen, M.F., and Popelar, C.H.: "Advanced Fracture Mechanics." Oxford University Press, New York, 1985.

[47] "Design Criteria for Controlling Stress Corrosion Cracking," MSFC–SPEC–522B, Marshall Space Flight Center, 1987.

[48] Osgood, C.C.: "Assuring Component Life." Machine Design, p. 95, September 2, 1971.

[49] "Standard NDE Guidelines and Requirements for Fracture Control Programs," MSFC–STD–1249, Marshall Space Flight Center, 1985.

[50] Parker, A.P.: "The Mechanics of Fracture and Fatigue." E.&F.N. Spon Ltd., New York, 1981.

[51] "Fracture Control Program Requirements," MSFC–HDBK–1453, Marshall Space Flight Center, 1987.

[52] "Fracture Control of Metallic Pressure Vessels," NASA SP–8040, NASA, May 1970.

[53] Hertzberg, R.W.: "Deformation and Fracture Mechanics of Engineering Materials." Second Edition, Wiley, New York, 1983.

[54] Srawley, J.E., and Esgar, J.B.: "Investigation of Hydrotest Failure of Thiokol Chemical Corporation 260–Inch Diameter SL–1 Motor Case," NASA TM X–1194, January 1967.

APPROVAL

Linear Elastic Fracture Mechanics Primer

By Christopher D. Wilson

The information in this report has been reviewed for technical content. Review of any information concerning Department of Defense or nuclear energy activities or programs has been made by the MSFC Security Classification Officer. This report, in its entirety, has been determined to be unclassified.

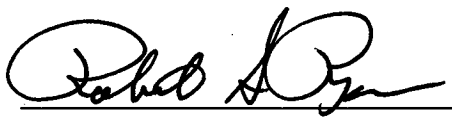

JAMES C. BLAIR
Director, Structures and Dynamics Laboratory

☆ U. S. GOVERNMENT PRINTING OFFICE 1992 – 631–060 / 60155

REPORT DOCUMENTATION PAGE

Form Approved
OMB No. 0704-0188

1. AGENCY USE ONLY *(Leave blank)*	2. REPORT DATE	3. REPORT TYPE AND DATES COVERED
	July 1992	Technical Memorandum

4. TITLE AND SUBTITLE
Linear Elastic Fracture Mechanics Primer

5. FUNDING NUMBERS

6. AUTHOR(S)
Christopher D. Wilson

7. PERFORMING ORGANIZATION NAME(S) AND ADDRESS(ES)
George C. Marshall Space Flight Center
MSFC, AL 35812

8. PERFORMING ORGANIZATION REPORT NUMBER

9. SPONSORING / MONITORING AGENCY NAME(S) AND ADDRESS(ES)
National Aeronautics and Space Administration
Washington, DC 20546

10. SPONSORING / MONITORING AGENCY REPORT NUMBER
NASA TM - 103591

11. SUPPLEMENTARY NOTES
Prepared by Structures and Dynamics Laboratory,
Science and Engineering Directorate

12a. DISTRIBUTION / AVAILABILITY STATEMENT
Unclassified-Unlimited

12b. DISTRIBUTION CODE

13. ABSTRACT *(Maximum 200 words)*

This primer is intended to remove the "blackbox" perception of fracture mechanics computer software by structural engineers. The fundamental concepts of linear elastic fracture mechanics are presented with emphasis on the practical application of fracture mechanics to real problems. Numerous "rules of thumb" are provided. Recommended texts for additional reading, and a discussion of the significance of fracture mechanics in structural design are given. Griffith's criterion for crack extension, Irwin's elastic stress field near the crack tip, and the influence of small-scale plasticity are discussed. Common stress intensity factor solutions and methods for determining them are included. Fracture toughness and subcritical crack growth are discussed. The application of fracture mechanics to damage tolerance and fracture control is discussed. Several example problems and a practice set of problems are given.

14. SUBJECT TERMS	15. NUMBER OF PAGES
brittle fracture, cracks, damage tolerance, fatigue crack growth, fracture control, fracture mechanics, stress intensity factors	78
	16. PRICE CODE NTIS

17. SECURITY CLASSIFICATION OF REPORT	18. SECURITY CLASSIFICATION OF THIS PAGE	19. SECURITY CLASSIFICATION OF ABSTRACT	20. LIMITATION OF ABSTRACT
Unclassified	Unclassified	Unclassified	